The establishment of a pelagic *Sargassum* population in the tropical Atlantic: Biological consequences of a basin-scale long distance dispersal event

Elizabeth M. Johns[a,*], Rick Lumpkin[a], Nathan F. Putman[b], Ryan H. Smith[a], Frank E. Muller-Karger[c], Digna T. Rueda-Roa[c], Chuanmin Hu[c], Mengqiu Wang[c], Maureen T. Brooks[d], Lewis J. Gramer[a,e], Francisco E. Werner[f]

[a] *Atlantic Oceanographic and Meteorological Laboratory, National Oceanic and Atmospheric Administration, Miami, FL 33149, USA*
[b] *LGL Ecological Research Associates, Inc., Bryan, TX 77801, USA*
[c] *College of Marine Science, University of South Florida, St. Petersburg, FL 33701, USA*
[d] *University of Maryland Center for Environmental Science, Horn Point Laboratory, Cambridge, MD 21613, USA*
[e] *Cooperative Institute for Marine and Atmospheric Studies, Rosenstiel School of Marine and Atmospheric Science, University of Miami, Miami, FL 33149, USA*
[f] *NOAA Fisheries, 1315 East-West Highway, Silver Spring, MD 20910, USA*

ARTICLE INFO

ABSTRACT

Starting in 2011, coastal areas of the Caribbean Sea and tropical Atlantic Ocean began to experience extraordinary yearly accumulations of pelagic *Sargassum* brown alga. Historical reports place large quantities of *Sargassum* only in the North Atlantic (mostly in the Gulf of Mexico and the Sargasso Sea). Accumulations of *Sargassum* in the tropical Atlantic have continued. We used a numerical particle-tracking system, wind and current reanalysis data, drifting buoy trajectories, and satellite imagery to determine the origin of the *Sargassum* that is now found persistently in the tropical Atlantic. Our analyses suggest that during the extreme negative phase of the winter 2009–2010 North Atlantic Oscillation (NAO), unusually strong and southward-shifted westerly winds explain the transport of *Sargassum* from the Sargasso Sea (∼20–40°N, 80–20°W) into the far eastern North Atlantic. Our hindcast *Sargassum* distributions agree with surface current simulations with the inclusion of "windage". Windage is the additional, wind-induced drift of material floating at the free surface resulting from direct wind forcing on the sea surface, as well as on floating or partially-submerged objects. In our simulations, windage is included as an added vector (speed and direction) to the model-computed surface ocean currents equivalent to 1% of surface wind velocities. Lagrangian analysis of the regional circulation suggests that (1) part of the *Sargassum* subsequently drifted to the southwest in the North Equatorial Current (NEC) and entered the central tropical Atlantic, arriving in the Caribbean by the spring of 2011, with (2) another portion continuing southward along the coast of Africa in the Canary Current, eventually joining the seasonally-varying system of tropical Atlantic currents and thereby delivering a large *Sargassum* population to the tropical Atlantic. Since then, *Sargassum* patches aggregate from March to September in massive windrows along the Inter-Tropical Convergence Zone (ITCZ) under the action of converging winds. The windrows follow the ITCZ in its seasonal northward migration in the central tropical Atlantic. They are stretched across the central tropical Atlantic as the ITCZ crosses the latitude of the seasonal formation of the North Equatorial Counter Current (NECC). These patches and windrows are exposed to high sunlight and open-ocean upward flux of nutrients due to eddy and wind-driven mixing in the central tropical Atlantic. During the northern spring and summer, as the *Sargassum* drifts farther north with the ITCZ, large portions of the population are advected into the eastern Caribbean Sea. Some of these patches remain dispersed as the ITCZ migrates southward, and re-aggregate into new windrows as the ITCZ intensifies the following March-April. If wind mixing is strong and the mixed layer is deeper than about 50–60 m in the southern tropical Atlantic at this time, the *Sargassum* will bloom and form a massive windrow. Otherwise, the bloom will be inhibited. The extreme 2009–2010 NAO wind anomaly could be considered as triggering a biosphere "tipping point" that caused important ocean-scale ecosystem changes in the tropical Atlantic, with significant recurrent social and economic consequences. Understanding whether this new expanded geographic range of massive *Sargassum* blooms is temporary or whether it will revert to its pre-2009 distribution requires sustained monitoring and research.

* Corresponding author.
  E-mail address: libby.johns@noaa.gov (E.M. Johns).

1. Introduction

The brown alga of the genus *Sargassum* inhabits tropical and subtropical waters around the world. In the Atlantic Ocean, there are more than 60 benthic species of *Sargassum* (Connor and Adey, 1977; Hanisak and Samuel, 1987; Martin, 2016) and two common pelagic species, *S. natans* and *S. fluitans* (Collins, 1917; Parr, 1939). In 2011, unusually large quantities of pelagic *Sargassum* began landing on the shores of islands of the Caribbean Sea, the Caribbean coasts of Central America and Mexico, and on the Atlantic coastline of tropical West Africa

(Gower et al., 2013). Such large quantities of *Sargassum* have occurred almost every year since then (Fig. 1d), forming what Wang et al. (2019a) called the "great Atlantic *Sargassum* belt". Because of the socio-economic impacts of the coastal inundations of *Sargassum*, many studies have focused on understanding the sudden, and now recurring, appearance of the blooms (e.g., Johnson et al., 2012; Gower et al., 2013; Smetacek and Zingone, 2013; Franks et al., 2016; Sissini et al., 2017; Djakouré et al., 2017; Lamb, 2018; Wang et al., 2019a; Oviatt et al., 2019). Several of these studies suggest that the *Sargassum* blooms have been due to anomalous nutrient discharge via the Amazon River related
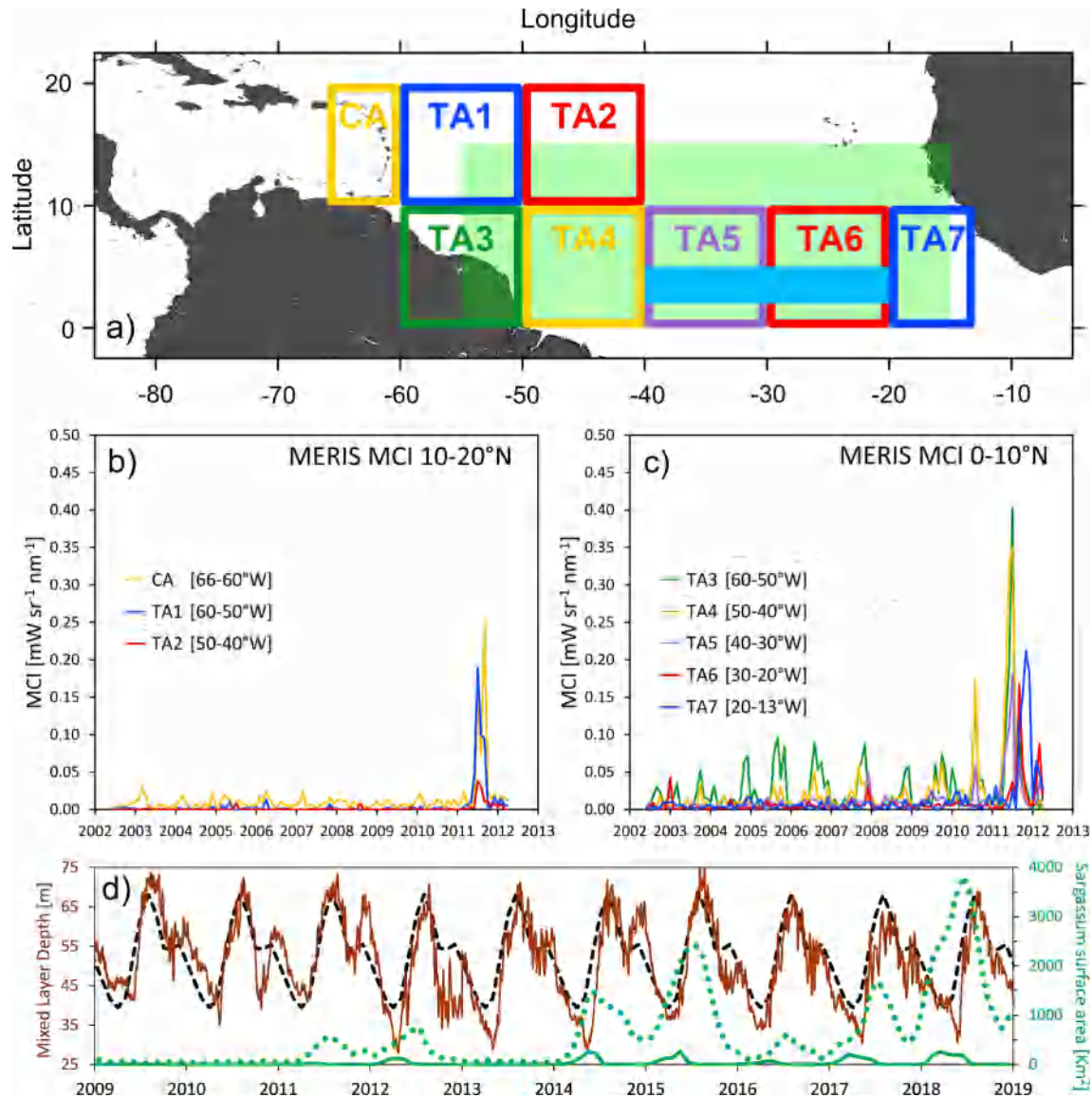

Fig. 1. Time series of *Sargassum* area coverage from satellites and Mixed Layer Depth (MLD) in the tropical Atlantic. Fig. 1a. Boxes used to compute the historical Maximum Chlorophyll Index (MCI) derived from MERIS satellite data shown in Fig. 1b and c. The green shaded rectangle and the smaller blue shaded rectangle were used to extract the central tropical Atlantic *Sargassum* area coverage from the MODIS satellite data shown in Fig. 1d. The nominal location of the Sargasso Sea from Laffoley et al. (2011) is shown as a black oval. Fig. 1b. Monthly mean MCI [units of radiance mW sr^{-1} nm^{-1}] in boxes between 10 and 20°N (data from Gower et al., 2013; Brooks et al., 2018). Fig. 1c. MERIS MCI averages for 0–10°N boxes. The sudden increase of *Sargassum* in the eastern equatorial Atlantic beginning in 2011 is observed in all areas, but it was observed first in 2010 in the 0–10°N band (boxes TA3, TA4, and TA5). Fig. 1d. Monthly mean *Sargassum* area coverage (km^2; data from Wang et al., 2019a, 2019b) in the region 0-15°N, 15-55°W (dotted green line; area corresponds to the green broken line shaded rectangle in Fig. 1a. Note that the *Sargassum* surface cover estimates shown in Wang et al. (2019a) are for a larger region: 5°–25°N, 15°E–89°W). Monthly mean *Sargassum* area coverage (km^2) in the region 2–5°N, 20–40°W (solid green line; blue shaded rectangle in Fig. 1a) and daily MLD (m) averaged over the region 2–5°N, 20–40°W (brown line; source: ECCO2 model; blue shaded rectangle in Fig. 1a) with MLD climatology (1992–2018) for the same region (black broken line).

to deforestation upstream, changes in upwelling off northwest Africa, changes in open-ocean upwelling, changes in the amount or deposition patterns of African dust, higher sea surface temperatures, or are the result of all of these causes combined (e.g., Sissini et al., 2017; Oviatt et al., 2019; Wang et al., 2019a). However, none of these studies explained the sudden appearance of *Sargassum* in the tropics or the continued annual recurrence of massive *Sargassum* blooms.

In this study, we propose a mechanism and pathways to address two main hypotheses. The first is that *Sargassum* was transported from the Sargasso Sea to the tropical Atlantic by anomalous winds in 2009–2010. The second is that the seasonal recurrence of *Sargassum* blooms in the central tropical Atlantic is the result of physical aggregation and biological growth due to local, open-ocean nutrient supply. These mechanisms explain the 2011 onset and the annual recurrence of the great trans-Atlantic *Sargassum* belt between about February and September, its weakening or dissipation between November and January, and the absence of a major *Sargassum* bloom in the tropical Atlantic in 2013 (Fig. 1d).

Our approach was to examine long distance dispersal pathways, aggregation mechanisms, and nutrient sources using six independent lines of evidence. Specifically, we used (1) results from numerical circulation models for surface ocean particle tracking, circulation, and vertical mixing, (2) wind and current reanalysis data, (3) individual and ensemble trajectories of drogued and undrogued drifting buoys, (4) historical time series of net tow collections of *Sargassum*, (5) synoptic satellite ocean color *Sargassum* observations, and (6) historical hydrographic observations. These six lines of evidence reveal the underlying reasons for the expansion in the geographic range of the *Sargassum* and for the subsequent recurrent seasonal aggregations in the tropical Atlantic.

We suggest that the "tipping point" of the *Sargassum* biogeography in 2011 is due to the long-range transport of *Sargassum* and the presence of local nutrient supplies in the central tropical Atlantic. Such a change in the biogeography of a species can have profound impacts on the ecology of a region (Smith et al., 2018; Duffy et al., 2019). Tipping points mark discontinuous changes in the state of an ecosystem that occur when external conditions reach thresholds that trigger an accelerating transition to a contrasting new state (e.g., van Nes et al., 2016; Dakos et al., 2019; and references therein). Tipping points can occur at population and community levels, and at ecosystem scales, and can incur long-term disruption to vital ecosystem services. Whether the new state for the Atlantic *Sargassum* distribution is permanent, leads to other continuing changes, or reverts to an earlier ecosystem state, is impossible to predict at this stage.

In essence, we now have a new and separate population of *Sargassum* in the tropical Atlantic that flourishes seasonally in a favorable habitat with higher sunlight, warmer temperatures, and higher nutrient availability than its sister population in the North Atlantic. As we describe below, the winds of the tropical Atlantic are the physical mechanism that aggregates the large blooms. Winds and currents then seasonally advect these blooms into the Caribbean (Johnson et al., 2012; Franks et al., 2016; Putman et al., 2018). The expansion in the geographic range of *Sargassum* will thus likely continue to have socioeconomic implications for human coastal communities downstream.

We find that the new annual *Sargassum* accumulations and blooms need not be caused or supported only by discharges of the Amazon River, northwest Africa upwelling, or equatorial upwelling, all of which are distant from the areas of the *Sargassum* accumulations during most of the year. Rather, the patches and windrows of *Sargassum* in the tropical Atlantic bloom in response to the high sunlight and open-ocean upward diffusive flux of nutrients due to eddy and mixed layer dynamics that they encounter there.

In Section 2 we provide background information on the distribution and abundance of *Sargassum* in the surface Atlantic Ocean, the climatological Atlantic winds and surface currents, the North Atlantic Oscillation (NAO), and the role of windage in defining the *Sargassum*'s

changing distribution. Section 3 explains the methods used, and Section 4 describes the results. Section 5 is an in-depth discussion of our findings. Section 6 summarizes our conclusions and highlights several remaining questions.

2. Background

2.1. Historical Sargassum distribution and its presence in the tropical Atlantic since 2011

The Sargasso Sea has been known to mariners for hundreds of years. Early sailors developed nightmare scenarios of monsters lurking in the Sargasso Sea, where sailing vessels could be caught in the midst of massive floating mats of *Sargassum* weed during wind lulls and become "ghost ships" (Dixon, 1925; Lamb, 2018). In some of the earliest scientific research on the Sargasso Sea, Collins (1917) described pelagic *Sargassum* as an alga that can spread by active vegetative growth of fragments dispersed by action of the wind at the surface of the ocean, and described massive pile-ups of *Sargassum* along the beaches of Bermuda. Similarly, Webster and Linton (2013) chronicle reported episodic occurrences of *Sargassum* along the Texas Gulf coast since the late 1800′s. Parr (1939) identified the two most abundant pelagic *Sargassum* species found in the Sargasso Sea, *S. natans* and *S. fluitans*. Using specially-designed nets, Parr (1939) demonstrated that nearly all the pelagic *Sargassum* floats at or very near the surface, and that it accumulates due to the action of the wind, often aggregating into long windrows (Coston-Clements et al., 1991; Witherington et al., 2012; Sanchez-Rubio et al., 2018).

Gower and King (2008) described the first Atlantic basin-wide coverage of *Sargassum* using the MEdium Resolution Imaging Spectrometer (MERIS) satellite (see also Gower et al., 2006). Gower and King (2011) studied the distribution of *Sargassum* using time series of ocean color satellite images. Their observations provided strong quantitative evidence that the largest populations of pelagic *Sargassum* were found in the Sargasso Sea and the Gulf of Mexico.

Gower et al. (2013) mapped the anomalous appearance of large amounts of *Sargassum* in the tropical Atlantic in 2011 and found that this population spanned the Atlantic basin from West Africa to northeast Brazil and the Caribbean Sea. They remarked that such distributions had not been seen previously in the tropical Atlantic. Fig. 1b, created from their data after averaging within latitude-longitude boxes (Fig. 1a), shows details of the timing of the *Sargassum*'s original arrival in the Caribbean. The MERIS data also show the first appearance of large amounts of *Sargassum* in the tropical western Atlantic in the second half of 2010 (Fig. 1c).

Franks et al. (2011) reported the many local impacts of the anomalous, massive arrival of *Sargassum* throughout the Caribbean Sea in 2011 on fishing, reef and benthic communities, mangroves, turtle hatchlings, and tourism. They used a numerical model to backtrack the Caribbean *Sargassum* accumulations to the tropical Atlantic, but found no direct or indirect linkage to the Sargasso Sea.

Since 2011, annual seasonal increases in *Sargassum* abundance have been observed in the tropical Atlantic using NASA's MODIS satellite sensors (Wang and Hu, 2016, 2017; Fig. 1d). Wang et al. (2019a) derived monthly distribution maps of *Sargassum* abundance for the Atlantic Ocean, Caribbean Sea, and Gulf of Mexico for 2000–2018. They documented the recurrence of the great Atlantic *Sargassum* belt every year since 2011 except for 2013, a year when the *Sargassum* did not form these accumulations in the tropical Atlantic. This belt often extended from West Africa to the Gulf of Mexico during summer months, with highest densities between approximately May and September (Wang et al., 2019a). They found evidence of small amounts of pelagic *Sargassum* in the satellite data of the tropical Atlantic prior to 2011, but no large aggregations (Fig. 1d).

Wang et al. (2019a) examined a number of factors in an effort to explain the development of the *Sargassum* aggregations observed since

2011 in the tropical Atlantic. They suggested that ocean circulation and variations in nutrient sources (Amazon discharge, coastal upwelling off West Africa, and equatorial upwelling), together with sea surface temperature variability, could explain the interannual changes in the amount of *Sargassum* observed. They proposed that the recurrent blooms might continue in future years because the increased populations now observed in the tropical Atlantic would serve as seeds for blooms in subsequent years.

2.2. Winds, currents and hydrography of the tropical and temperate North Atlantic Ocean

The climatological winds over the tropical and temperate North Atlantic are dominated by the westerlies and the trade winds (Fig. 2a). The westerlies blow from the US and Canadian east coasts north of ~30°N toward the northeast and across the North Atlantic. The northeast trade winds blow westward, from Africa, between the equatorial region and ~25°N (e.g., Sverdrup et al., 1942; Stewart, 2008). The center of the wind rotation formed by the westerlies and the northeast trade winds is on average located over the Sargasso Sea, between Bermuda and the Azores islands. In general, average winds along the US southeast coast are weak and northward. On the east side of the Atlantic, on average, stronger southward winds occur off Gibraltar and the Iberian Peninsula (Spain and Portugal). Winds along the coast of northwest Africa are to the south and strongly seasonal. In the tropics, the southeast trade winds converge with the northeast trade winds (Fig. 2a) to form the Inter-Tropical Convergence Zone (ITCZ). The ITCZ features an annual excursion from its southernmost location (~3°N) around February-March to about 11°N in August, when it starts moving southward again (Colna, 2017).

The large-scale North Atlantic Ocean surface circulation is dominated by a subtropical gyre (Fig. 2b). The Gulf Stream defines the western side of the gyre, and its extension crosses the northeastern Atlantic. There, the circulation branches to the north as the North Atlantic Current and to the south as the Azores and Canary Currents. The Canary Current (CC) also splits, with one branch turning westward as the NEC and the other continuing south along the West Africa coast. The South Equatorial Current (SEC) flows from the eastern South Atlantic across the Atlantic basin toward equatorial Brazil. Part continues to the south along the coast of Brazil, and part flows along the northeast coast of South America as the North Brazil Current (NBC), which continues as the Guiana Current (GC). These waters, and those of the NEC, enter the Caribbean Sea to form the Caribbean Current (CA).

The Caribbean Current continues into the Gulf of Mexico as the Yucatan Current, which then becomes the Loop Current (LC), and continues as the Florida Current until it merges with waters from the NEC to form the Gulf Stream, completing the subtropical gyre surface circulation (Sverdrup et al., 1942; Stewart, 2008; and others).

The surface circulation of the tropical Atlantic is complex and seasonal, driven by the seasonally-varying winds including the north-south migration of the ITCZ. Every May, the North Equatorial Counter Current (NECC) forms, and the NBC separates from the coast, retroflects, and flows eastward, joining the NECC (Muller-Karger et al., 1988, 1995; Richardson et al., 1992; Lumpkin and Garzoli, 2005). The retroflection advects the Amazon River plume offshore into the NECC (Muller-Karger et al., 1988, 1995). Large rings form quasi-periodically from the NBC retroflection and move to the northwest, also carrying Amazon River plume water (Bruce, 1984; Johns et al., 2014).

To the east, the Atlantic off West Africa between 10 and 16°N is an area of interactions between the CC, the NEC, and the NECC. Upwelling off Mauritania–Senegal shows a maximum between about December and June (e.g., Sánchez-Garrido et al., 2019, and references therein). Between about 5–10°N, at ~20°W there is a major cyclonic ocean circulation feature known as the Guinea Dome (Fig. 2a; Mittelstaedt, 1991; Stramma and Schott, 1999). Seasonal upwelling occurs along the equator, with maxima between June and September every year which are driven by complex dynamics (Weisberg and Tang, 1985, 1990; Weisberg and Colin, 1986; Weingartner and Weisberg, 1991; Carton and Zhou, 1997; Grodsky et al., 2008; Wang et al., 2017; Foltz et al., 2019).

Many of the convergences and divergences in the upper layer of the tropical Atlantic are caused by seasonal spatial variations in the wind. In addition to the complex system of horizontal zonal currents mentioned above, Ekman pumping and Ekman divergence and convergence (c.f. Chereskin and Price, 2001; Inui et al., 2002; Kessler, 2006) lead to areas of open-ocean upwelling and downwelling that migrate north and south with the changing winds. Indeed, while the ITCZ is an area of wind convergence, it is also associated with weak but positive Ekman pumping (open-ocean upwelling), driven by the curl of the wind across a large section of the tropical Atlantic (Schott et al., 2004; see details in Section 4.5.2 below). This band is slightly offset to the north of the ITCZ. Between about February and July, this region of positive Ekman pumping moves seasonally over an area of seasonally raised isotherms (with the 20 °C isotherm reaching < 50 m) that represents the cyclonic boundary between the NECC and the NEC (Katz, 1981; Reverdin et al., 1991). The zonal band of positive Ekman pumping migrates through
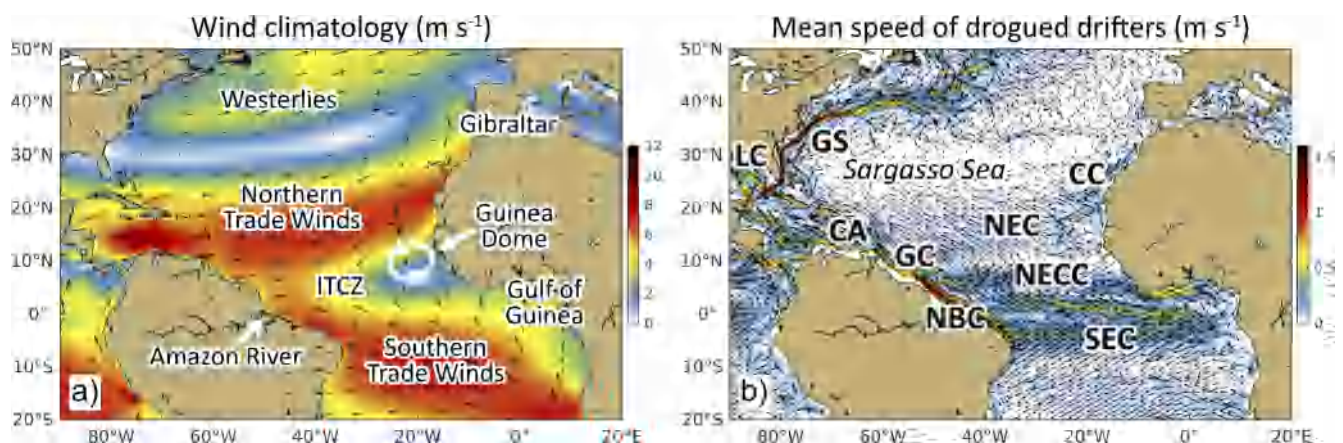

Fig. 2. (a) Climatological winds over the North Atlantic Ocean, showing the westerlies, the northern and southern trade winds, and the climatological location of the seasonally-varying Inter-Tropical Convergence Zone (ITCZ). Data are averaged over the period January 1979 through December 2017, from ERA-Interim winds. (b) Climatological surface currents of the Atlantic Ocean from satellite-tracked surface drifters drogued at 15 m depth, showing the Sargasso Sea, the major currents forming the subtropical gyre: the Gulf Steam (GS), Canary Current (CC), North Equatorial Current (NEC), Caribbean Current (CA), and the Loop Current (LC), and the locations of the seasonally-varying tropical Atlantic currents: the North Equatorial Counter Current (NECC), South Equatorial Current (SEC), North Brazil Current (NBC), and the Guiana Current (GC). Data are averaged over the period January 1979 through July 2018.
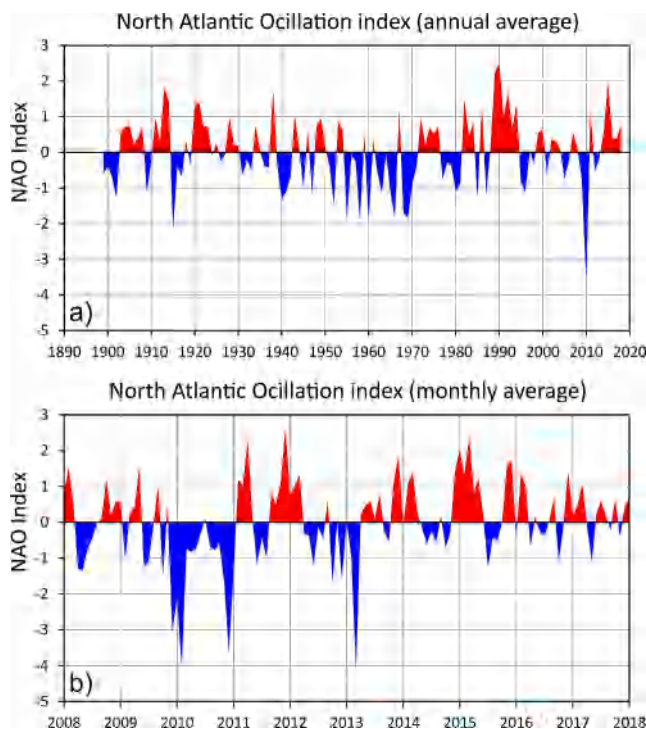
Fig. 3. (a) The annual average of the North Atlantic Oscillation (NAO) index for the time period 1899 to 2018. Calendar year 2010 was the most extreme annually-averaged negative NAO event observed in the 100 + year record. (b) The monthly average of the NAO index for the time period 2008 through 2018. Three negative NAO events are evident, during winter 2009–2010, December 2010, and March 2013. Data were obtained from https://climatedataguide. ucar.edu/climate-data/hurrell-north-atlantic-oscillation-nao-index-pc-based for (a) and (b).

the region between about 2°N and 10°N with the ITCZ, where mixed layers > 50–80 m are typical for July-December, < 50 m starting in January, and as shallow as < 30 m each May (e.g., Kara et al., 2003; Montégut et al., 2004; see Fig. 1d, Section 3.1.2 and the results in Section 4.5.2 below). In August-October, the area of positive Ekman pumping moves farther to the north of the ITCZ, over waters with deeper mixed layers, where the 20 °C isotherm is typically deeper than 100 m.

2.3. The North Atlantic Oscillation

The North Atlantic Oscillation (NAO) is a quasi-periodic oscillation of the sea level pressure difference between the Azores High and the Icelandic Low (Hurrell and Deser, 2009). The variation of this pressure difference, on time periods of months to years, shifts the north-south location of the Jet Stream, which in turn drives changes in the large-scale wind field and ocean surface currents over the entire North Atlantic Ocean. During its positive phase, the NAO is associated with a northward shift of the westerlies, strengthened trade winds, and milder winters in the eastern US and Europe. During its negative phase, the NAO is associated with a southward shift of the westerlies, weakened trade winds, and cold winter temperatures with increased winter precipitation in the eastern US and Europe (Schmitt, 2000).

A time series of the NAO index was obtained from NOAA's Climate Prediction Center (https://climatedataguide.ucar.edu/climate-data/ hurrell-north-atlantic-oscillation-nao-index-pc-based). The annual average from 1899 through 2018 is shown in Fig. 3a. The NAO index reached its lowest annual average since 1899 during calendar year 2010. Fig. 3b shows the monthly average NAO index from 2008 through 2018. Three major negative NAO events occurred during this period: December 2009 through March 2010, December 2010, and

March 2013. The winter 2009–2010 event was strong and persisted over several months. The December 2010 and March 2013 events each lasted only one month and followed several months of weaker negative NAO values.

2.4. The role of windage

Sargassum drifts in the surface ocean under the influence of the wind (Collins, 1917; Parr, 1939; Blomquist and Pyron, 1943; Glynn et al., 1964; Winston et al., 1997; Moreira and Alfonso, 2013; Gavio et al., 2015). Studies using drift cards, standard ship drift records, drifting buoys, drifting oil patches (e.g., Hughes, 1956; Tomczak, 1964), and an abandoned derelict sailboat (Brown, 1991) have demonstrated that (neglecting for a moment the ocean currents) floating objects tend to move downwind at a speed proportional to, but much smaller than, the speed of the wind (generally 1 to 3% of the wind speed). The exact percentage depends on the physical characteristics of the floating object, how much of it is submerged, and the magnitude of the wind speed. Herein, we refer to "windage" as the added direct wind forcing at the sea surface, including all wind forcing on the water as well as on the floating object (Allshouse et al., 2016).

Drogued and undrogued surface drifters provide important quantitative information about windage. Lumpkin and Pazos (2007) found that undrogued near-surface drifters experience a windage factor of about 1% in the direction of the wind. For drifters drogued at 15 m depth, this effect is approximately an order of magnitude smaller. Lumpkin et al. (2013) attributed the difference in the movement of drogued vs. undrogued drifters to a combination of wind drag on the surface float, the vertical shear of wind-driven currents in the upper 15 m, and wave-induced Stokes drift.

In our simulations, windage is an added vector (speed and direction) used to compute the *Sargassum*'s trajectories in space [$\mathbf{x}$; where $\mathbf{x}$ is the position vector with coordinates (x, y, z)] and time (t). Specifically, the effective surface velocity $\mathbf{u}_s$

$$\mathbf{u_s}(\mathbf{x},\, t) = \mathbf{u_m}(\mathbf{x},\, t) + C_w \mathbf{u_w}(\mathbf{x},\, t)$$

is the sum of $\mathbf{u}_m$, the velocity obtained from the circulation models (see Sections 3.1.1 and 3.2.1), and $\mathbf{u}_w$, the wind velocity at 10 m above the ocean's surface modulated by the windage coefficient C_w (for which we conducted sensitivity studies in the 0.01 to 0.03 range, comparable to Allshouse et al., 2016).[1]

Most operational methods utilized to track floating marine objects add a similar windage factor to synoptic surface-layer currents, such as those generated by numerical models (NOAA, 2016). Recently, Putman et al. (2018) successfully predicted *Sargassum* influxes to the Caribbean Sea from the tropical Atlantic on seasonal to annual time scales by explicitly including windage as described above. Herein we implement a similar strategy to identify possible distant sources of the *Sargassum,* by examining particle trajectories in the North and South Atlantic over several years prior to 2011 under the influence of synoptic surface winds and ocean currents.

3. Data and methods

A description of each of the six independent methods used to develop evidence to test our two core hypotheses follows.

---

[1] We have assumed a constant windage coefficient C_w. However, *Sargassum* has been shown to sink in the presence of Langmuir cells and wind speeds ~5 m/s and higher (Johnson and Richardson, 1977). In these cases, C_w should be expected to decrease. We are not aware of studies that explicitly consider the dependence of C_w on wind speed and on the type of floating material. Our simulations with a range of values of C_w are a way of approximating different levels of windage.

3.1. Numerical models

3.1.1. The HYCOM/ICHTHYOP numerical model

We analyzed surface-layer currents from the data-assimilating Global HYbrid Coordinate Ocean Model (HYCOM; Chassignet et al., 2007) in conjunction with the ICHTHYOP Lagrangian particle tracking model (Lett et al., 2008). Global HYCOM is an eddy-resolving model that assimilates selected *in situ* and satellite observations to characterize past oceanic conditions. Daily Global HYCOM hindcasts are provided at a spatial resolution of 0.08° not including windage at the sea surface, which is nominally the average over the upper 2 m of the water column (https://www.hycom.org/). ICHTHYOP is a free Java tool designed to study the effects of physical and biological factors on ichthyoplankton dynamics (https://www.ichthyop.org/). The tool uses as input time series of velocity, temperature and salinity fields.

Putman et al. (2016) found greater qualitative agreement between Global HYCOM surface currents and the trajectories of drifters drogued at 15 m depth than with undrogued drifters. Based on this result, and assuming that *Sargassum* at the sea surface moves more like undrogued drifters than drogued drifters, we included a 1% windage correction to HYCOM's surface currents, by adding 1% of the wind speed in the direction of the wind. Using NCEP reanalysis wind data (see Section 3.2.1 below), we ran experiments with both no windage correction and with a 1% windage correction.

3.1.2. The ECCO2 numerical model

To consider the role of subsurface nutrient supply, we examined temporal changes in the tropical Atlantic Ocean's Mixed Layer Depth (MLD). Numerical simulations provide an alternative to limited field measurements for assessment of variability in the mixed layer (c.f. Muller-Karger et al., 2015). We used MLD estimates from the ECCO2 (*Estimating the Circulation and Climate of the Ocean, Phase II*; Menemenlis et al., 2008; Wunsch et al., 2009) Cube 92 model results (https://ecco.jpl.nasa.gov/drive/files/ECCO2/cube92_latlon_quart_90S90N/). Results obtained from the NASA Jet Propulsion Laboratory ECCO project had daily temporal resolution, 1/4° horizontal resolution, and a vertical resolution of 10 m for the upper ocean from 1992 to 2019. Daily average MLD was estimated as the depth at which the potential density relative to the surface is larger than surface density by using the DeltaRho = 0.8 °C *Alpha criterion, where Alpha is the thermal expansion coefficient at the surface (Kara et al., 2000). Monthly time series and climatologies were derived from the time series of daily estimates.

3.2. Surface wind and ocean current data

Depending on the objectives, we used two different sets of wind and of ocean currents at different temporal and spatial resolution.

3.2.1. Reanalysis wind and current data

Monthly wind data, at 2.5° degree of spatial resolution, were obtained from the National Centers for Environmental Prediction (NCEP)/National Center for Atmospheric Research (NCAR) reanalysis (Kalnay et al., 1996; Kistler et al., 2001).

Monthly surface current data (at 5 m depth) with 1/3° degree of spatial resolution were obtained from the NCEP Global Ocean Data Assimilation System (GODAS). The GODAS model is forced by the momentum, heat, and fresh water flux output of the NCEP/NCAR reanalysis including wind, temperature, and salinity. Both the NCEP reanalysis winds and GODAS current data can be found at http://www.esrl.noaa.gov/psd/.

Methods used in the analysis of the NCEP wind and surface current data include spatial mapping and comparisons between the climatological patterns (as defined in this case by the 2008–2015 time period) and the winter 2009–2010 NAO negative anomaly period (as defined in this case by January-March 2010). We show maps of the surface currents with and without a 1% windage correction, and maps of both the

wind and current anomalies associated with the January-March 2010 NAO event. We also generated time series of the winds and currents averaged over 20–40°N, 20–80°W, which encompasses the Sargasso Sea and the area to its east, and examined the difference in the surface currents with and without the windage correction (discussed in Section 4.2 below).

3.2.2. Cross-Calibrated Multi-Platform (CCMP) wind product

Higher resolution surface winds (6-hours, 0.25° lat/lon resolution, referenced to 10 m above sea level) were used to derive a time series of wind divergence and the position of the ITCZ, and to estimate open-ocean upwelling vertical velocity due to Ekman pumping (Chereskin and Price, 2001; Schott et al., 2004). We used gridded zonal and meridional 5-day satellite winds available as the Cross-Calibrated Multi-Platform (CCMP) product from the NASA MEaSUREs project (NASA/GSFC/NOAA 2009; Making Earth Science Data Records for Use in Research Environments; NASA Jet Propulsion Laboratory Physical Oceanography Distributed Active Archive - JPL PO-DAAC; https://doi.org/10.5067/CCF30-01XXX). The CCMP datasets combine cross-calibrated satellite surface winds obtained from Remote Sensing Systems (REMSS) using a Variational Analysis Method (VAM) to produce this high-resolution gridded analysis (NASA/GSFC/NOAA 2009).

The ITCZ is a broad (> 300 km) region of convergence of the trade winds that spans the tropical Atlantic. We used the u and v wind components from the CCMP product to calculate wind divergence and traced the ITCZ position as the maximum in wind convergence (the negative of wind divergence) for the period July 1987 to December 2018, following the approach of Colna (2017). We recorded the latitudinal maximum of convergence every 0.25° of longitude and used these locations to trace the ITCZ position. This line thus represents an index of the broad region of convergence in the winds. A monthly climatology for the position of the ITCZ was derived for 2010–2018, the period concurrent with the higher *Sargassum* biomass in the tropical Atlantic (discussed in Section 4.5.2 below).

We also used the CCMP winds to estimate open-ocean upwelling rates. Vertical velocity due to Ekman pumping [m d^{-1}] was calculated by computing the wind stress components (Bakun 1973) using a drag coefficient fit to low and high wind speeds (Oey et al., 2006, 2007), and then the wind curl (Smith, 1968). Those calculations were done for each 6-hour wind map, and then averaged monthly.

3.2.3. The OSCAR circulation analysis

To examine wind and ocean surface current interactions in the central tropical Atlantic, we also examined results from the OSCAR (Ocean Surface Current Analysis Real-time) system. OSCAR contains a blend of near-surface ocean current estimates with sea surface height, surface vector wind, and sea surface temperature from various satellites and *in situ* instruments. The model formulation combines geostrophic, Ekman, and Stommel shear dynamics, and a complementary term from the surface buoyancy gradient (Bonjean and Lagerloef, 2002). Data are on a 1/3° grid with a 5-day resolution. OSCAR is generated by Earth & Space Research (ESR 2009; https://www.esr.org/research/oscar/). A monthly time series and climatology for the OSCAR surface currents was derived for 2010–2018 (discussed in Section 4.5.2 below).

3.3. Surface drifters

Data from the NOAA Global Drifter Program (https://www.aoml.noaa.gov/phod/gdp/) were used to examine how floating and partially-submerged objects respond to wind and ocean current forcing. The main body of a drifter is a surface float containing a sea surface temperature sensor, batteries, and a satellite transmitter. The drifter float is tethered to a "holey sock" drogue centered at 15 m depth. These drifters are deployed globally and tracked by satellite for periods of up to several years.

We used these data to examine the surface circulation of the North

and South Atlantic Ocean based on separately-averaged drogued and undrogued drifter data from 1979 to 2018. We calculated the statistical probability that drifters (drogued and undrogued) located in a 1° square grid cell would reach any other grid cell (Lumpkin et al., 2016). Next, using the observed drifters' statistics, a model was developed to simulate the spread (in either direction in time) of a near-surface tracer (Lumpkin et al., 2016). A time history was generated to examine details of the development of the inflow pathways of the tracer to the Caribbean at an initial 30-day time interval from launch to 30 days, and then a 60-day time interval thereafter, up to a maximum of 450 days. Finally, we examined individual drifter trajectories. These provided specific details of the connectivity between different regions of the Atlantic during 2010 through 2012.

3.4. Sargassum observations from net tows

Net tow data collected onboard the *SSV Corwith Cramer* operated by the Sea Education Association (SEA), with support from SEA faculty, staff, and SEA Semester students (SEA 2006–2016), were used to examine the time history of the distribution and abundance of specific types of pelagic *Sargassum* in the tropical Atlantic and Caribbean Sea (J. M. Schell, personal communication, 2017). These ship-based observations are not synoptic, and thus it is difficult to make quantitative inferences about seasonal and interannual variations of *Sargassum* because the sampling is limited to the location of the ship at any one time. This dataset is valuable for ground-truthing satellite-based observations of pelagic *Sargassum*, and to demonstrate that the *Sargassum* species observed in 2011 in the central tropical Atlantic were the same as those historically found in the Sargasso Sea.

The net tow samples were collected with a surface skimming neuston net (1 m wide × 0.5 m high, 333 μm mesh) towed at each station for approximately 1 nautical mile at 2 knots. Data are reported in grams of *Sargassum* species and sub-species collected per tow. The sum of the two most historically abundant sub-species (*S. natans I* and *S. fluitans III*) found in the Sargasso Sea was used in this analysis, and referred to in what follows as simply "*Sargassum*" unless otherwise noted.

Sargassum data from the net tow stations were examined within specific geographical boxes located in the Sargasso Sea, the tropical Atlantic, and the eastern and western Caribbean. A total of 1064 net tow stations collected between 2006 and 2016 (usually during the spring and fall) were used in our analysis; this is a subset of the total period over which these data were collected. Most of the net tow samples were collected in the Sargasso Sea between October 2006 and May 2016 (667 samples). The western Caribbean, eastern Caribbean, and tropical Atlantic had 92, 212, and 93 samples respectively, collected between October 2006 and April 2016. No averaging or other processing beyond dividing the stations into the four geographical groupings was done with the data.

3.5. Sargassum observations from satellite-derived remote sensing

We used two different datasets to examine the time history of pelagic *Sargassum* in the temperate and tropical North Atlantic Ocean.

3.5.1. MERIS satellite imagery
We used a product developed using the Medium Resolution Imaging Spectrometer (MERIS, of the European Space Agency), as these data were used to first detect the widespread redistribution of pelagic *Sargassum* in the tropical North Atlantic (Gower et al., 2013). A satellite-derived *Sargassum* index was obtained from the historical, daily level-1 radiances of the MERIS satellite sensor (the Maximum Chlorophyll Index, or MCI, as described in Gower et al., 2013; Brooks et al., 2018). The MCI takes advantage of the radiance peak at 709 nm, which is unique to the MERIS sensor, to detect concentrated surface blooms and floating vegetation. The spatial resolution of daily composite MCI is

5 km, recording the maximum MCI value for any 1.2 km pixel contained within each 5-km area.

Monthly time series of the MCI from 2002 to 2012 (the end of the MERIS data set) were averaged within large geographical boxes among two latitude ranges: three boxes between 10 and 20°N across the eastern Caribbean and in the western tropical Atlantic, and five boxes between 0 and 10°N spanning the tropical Atlantic closer to the equator (Fig. 1a). Although unable to differentiate between the two pelagic species of *Sargassum*, the MCI allowed for a temporal and spatial assessment of a wider area of the tropical Atlantic and Caribbean before and during the 2011 *Sargassum* arrival (Fig. 1b and c) than was possible using the much more limited SEA net tow data.

3.5.2. MODIS satellite imagery
We also used the new time series of surface ocean pelagic *Sargassum* distribution and density derived by Wang et al. (2019a, 2019b) using the NASA Moderate Resolution Imaging Spectrometers (MODIS) for a more complete analysis of its seasonal and interannual distribution (https://accession.nodc.noaa.gov/0190272). The MODIS observations extend the time series provided by MERIS. They are based on an objective method to account for variable observing conditions and partial pixel coverage. We used the series (2000–2018) of monthly surface cover maps to study the seasonal variability in the spatial aggregation patterns of *Sargassum* in the tropical Atlantic. We computed monthly mean *Sargassum* area coverage (km^2) for the region 0–15°N, 15°–55°W (note that the surface cover estimates shown in Wang et al. (2019a) are for the larger region 5°S–25°N, 15°E–89°W). The area coverage (km^2) represents pelagic *Sargassum* aggregated on the surface. Using the Wang et al. (2019a, 2019b) data, we also derived monthly climatological means (2010–2018) for *Sargassum* density and spatial distributions.

3.6. Hydrographic observations

Vertical profiles of salinity, temperature, and nutrients (nitrate, phosphate, silicate) for the tropical Atlantic were examined using the World Ocean Atlas WOA18 (National Oceanic and Atmospheric Administration; https://www.nodc.noaa.gov/OC5/woa18/). WOA18 aggregates field observations collected from multiple *in situ* platforms from the early 1900s to the present. We used the climatological objectively interpolated mean fields at 1° spatial resolution. While we examined all of these composite fields, here we highlight some of the findings using only the climatological nitrate data.

4. Results

4.1. Surface current and simulated particle drift patterns inferred from Global HYCOM model results

The initial wave of *Sargassum* entering the Caribbean Sea began in the spring of 2011 (Fig. 1b; see also Franks et al., 2016). In order to find the sources of that initial wave of *Sargassum*, we released 30,000 synthetic particles between April and June 2011 at random locations and at 5-day intervals throughout the Caribbean Sea, and backtracked them using surface currents from HYCOM and a 1% windage factor from NCEP reanalysis winds at 10 m above the ocean surface. This approach was identical to Putman et al.'s (2018) and Wang et al.'s (2019a) simulations. Putman et al. (2018) backtracked particles for 1 year, as their focus was on transport pathways from the Equatorial Atlantic to the Caribbean Sea. Wang et al. (2019a) backtracked particles for 6 months to examine the possible *Sargassum* connectivity across the entire Atlantic Ocean. Recent studies examining the potential for long distance connectivity in marine macrophytes have used tracking durations of > 3 years (e.g., Smith et al., 2018; Fraser et al., 2018). Hence, to examine whether longer tracking periods would influence Putman et al.'s (2018) and Wang et al.'s (2019a) results, in the present study we backtracked particles for 2 years (Fig. 4).
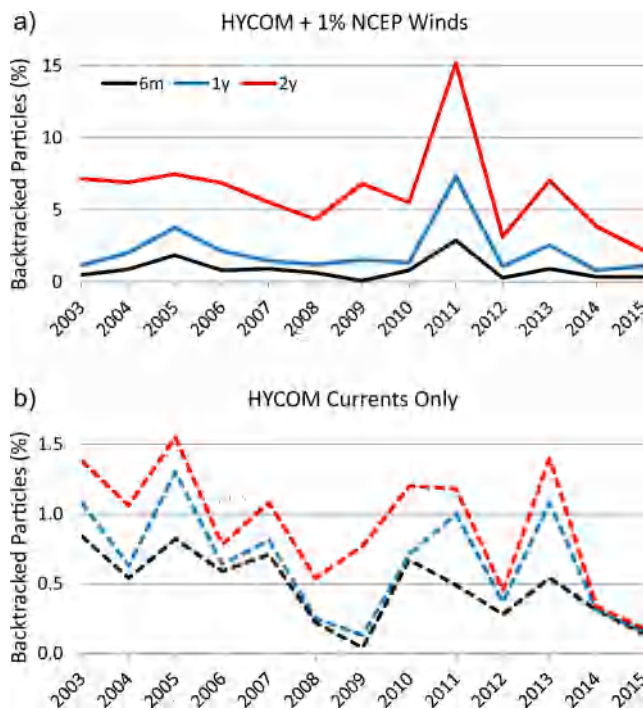

Fig. 5. Global HYCOM backtracking model results. Percentage of synthetic particles released across the Caribbean Sea in April-July of a given year that were backtracked to the North Atlantic (north of 23°N) within 6 months (black), 1 year (blue), and 2 years (red). (a) Results based on simulations using HYCOM surface currents and 1% windage from NCEP 10 m winds. (b) Results based on HYCOM surface currents only (i.e., no windage effect). Note the change of scale of the vertical axis.

speed. The long-term mean of the zonal velocity with no windage is small (0.01 +/− 0.01 m/s), with a range of just below zero to 0.05 m/s (where eastward velocity is positive). In contrast, the addition of windage of 1%, 2%, and 3% increases the current speed in both the positive and negative directions, yielding a larger range of zonal current speeds from −0.10 to 0.17 m/s. The highest positive values occurred during the three negative-NAO eastward wind anomaly time periods.

Fig. 10 shows the January-March 2010 anomaly of the winds and currents (with 1% windage), computed by subtracting the climatological values from the January-March 2010 values at each grid point. The wind anomaly (Fig. 10a) shows a large counter-clockwise circulation pattern spanning the Atlantic north of around 20°N. This pattern is typical of a negative NAO, although the magnitude is far larger (e.g., Fig. 3). South of ~10°N the anomaly wind field was near-zero.

The anomaly of the January-March 2010 currents with 1% windage (Fig. 10b) shows patterns similar to that of the January-March 2010 winds in the temperate North Atlantic, with an enhanced southward-shifted eastward flow all the way east to Gibraltar occupying the 30-40°N latitude band. Anomalous westward flow was observed north of 40°N. There were also relatively larger anomalies in the currents off northeast Brazil in the western tropical Atlantic, where the wind anomalies (Fig. 10a) were particularly small. These were due to a stronger than average NBC retroflection as well as variability due to NBC rings.

4.3. Surface current patterns inferred from a statistical drifter model and individual field-deployed drifter trajectories

4.3.1. Statistical drifter model
Drifters provide an independent, empirical check of the Global HYCOM and reanalysis surface current patterns. Maps of the climatological (1979–2018) surface currents in the North Atlantic based on

separated drogued and undrogued drifter data sets from 1979 to 2018 are shown in Fig. 11. In comparison to the climatological circulation patterns based on drogued drifters (Fig. 11a, also discussed earlier as Fig. 2b), the surface currents estimated from undrogued drifters show a strengthening of the subtropical gyres of the North and South Atlantic. There is a stronger southward and more organized flow in the undrogued drifter map near Gibraltar and in the Canary Current.

Fig. 12 illustrates the fraction of drogued and undrogued drifters from 1979 to 2018 that eventually entered the Caribbean Sea, regardless of the time that it took for them to do so. The results from the drogued drifters (Fig. 12a) are in very good agreement with those of Franks et al. (2011, 2016) and Johnson et al. (2012), who found that drogued drifters originated more typically in the western tropical Atlantic, with no direct connection with the Sargasso Sea to the north. On the other hand, the undrogued drifters (Fig. 12b) show a clear connection between the Caribbean and the eastern tropical Atlantic, from both the South Atlantic (by way of the Benguela Current as far south as 12°S along the coast of Africa), and from the North Atlantic (by way of the Canary Current from as far north as 30° to 40°N). In fact, the northern route is the dominant pathway for undrogued drifters to reach the Caribbean.

To add temporal information to the drifter results and to increase the robustness of these results, the evolution of a simulated tracer obeying observed drifter statistics is shown as a time series in Fig. 13. We backtracked simulated drifters at increments of 30–60 days over a period of 450 days, from an initial start position in the eastern Caribbean at 15°N, 64°W. In the short term (30 days), all the "drogued" tracer that reached the Caribbean originated in the western tropical Atlantic (Fig. 13a). At longer time scales, the "drogued" tracer reaching the Caribbean Sea can originate from the far eastern tropical Atlantic as well as the South Atlantic. At time scales > 270 days there was also a small probability of a source region from the western North Atlantic subtropical gyre.

Similarly to the "drogued" tracer, the "undrogued" tracer (Fig. 13b) originates in the western tropical Atlantic in the short term (30 days). At longer time scales (> 150 days) the "undrogued" tracer reaching the Caribbean can come from either the far eastern tropical Atlantic or the western South Atlantic. However, at > 270 days a pathway from Gibraltar along the coast of Africa in the Canary Current to the tropical Atlantic emerges. At even longer time scales (> 330 days), most of the "undrogued" tracer that eventually ends up in the Caribbean originates from off the coasts of Gibraltar, Spain, and Portugal and the coast of southern Africa in the South Atlantic. This "undrogued" tracer can take one year or longer to travel from Gibraltar to the Caribbean.

4.3.2. Individual field-deployed drifter trajectories
These patterns are corroborated by individual drifter trajectories that were located at sea during the anomalously negative NAO. Fig. 14a shows the trajectories of 23 drifters chosen to illustrate the range of pathways leading to the areas that experienced the 2011 *Sargassum* inundations, including West Africa between the equator and 10°N, northeast Brazil, and the Caribbean Sea. Overall, drifters that reached the eastern North Atlantic north of 30°N in 2011 came directly from the west between 30°N and 40°N. This is consistent with the eastward wind and surface current anomalies shown previously for January-March 2010. The major effect of the NAO wind anomaly was to enhance the chance of drifters escaping the subtropical gyre to the east toward Gibraltar and the coast of Africa. Once there, the Canary Current provides a direct connection to both southwestward flow in the NEC and southward flow toward the NECC and the rest of the tropical Atlantic.

Drifters selected for more detailed analysis and description are shown in colors in Fig. 14a. The northernmost drifter (number 83401, colored dark blue), was deployed in the Sargasso Sea on January 19, 2009 at 35.2°N, 58.1°W. This drifter lost its drogue only 3 days after deployment. It meandered in the northern half of the Sargasso Sea for almost a year, and then traveled east along ~39°N during the NAO
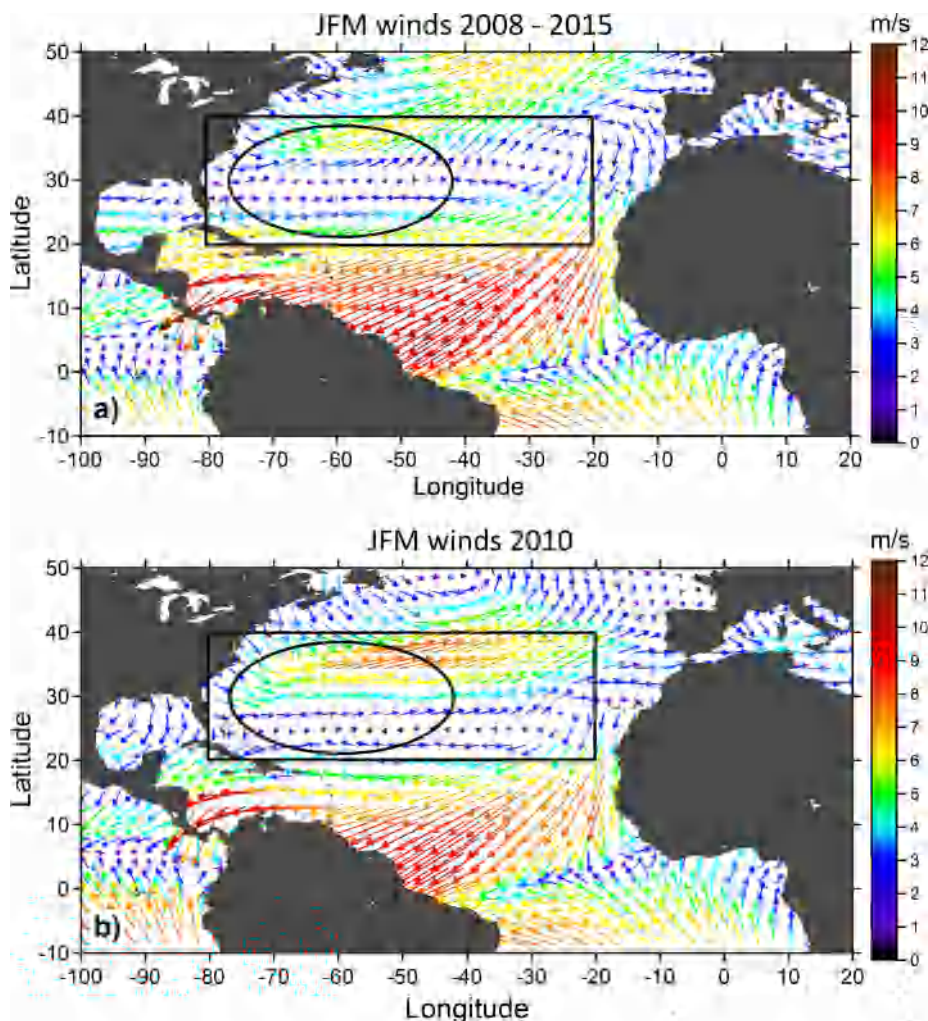
Fig. 6. (a) Climatological January-February-March (JFM) winds for 2008–2015. (b) JFM winds for 2010 from the NCEP monthly reanalysis data. Note in particular the winds in the 20–40°N, 80–10°W band (black rectangle), which encompasses the nominal Sargasso Sea (black oval). In the JFM 2010 map the westerlies are stronger and located farther south than the climatological winds. During JFM 2010 the eastward winds continue all the way to Gibraltar, whereas in the climatological map the winds are southward near Gibraltar. The nominal Sargasso Sea is shown as a black oval, after Laffoley et al. (2011).

wind event, from ~25°W to 13.1°W between December 1, 2009 and March 31, 2010 at an average speed of ~0.10 m/s (11.9 degrees of longitude in 121 days). This is consistent with the currents computed with 1% windage (Fig. 8b, light green tones; also Fig. 9b). Shortly after March 31, 2010 when the NAO anomaly ended, drifter 83,401 turned sharply to the south in the Canary Current, running aground on the coast near Morocco on July 4, 2010 (at ~28°N, 12.7°W). Two other drifters (83403, shown in gray, and 83404, shown in purple) followed similar trajectories and grounded in the same vicinity.

Drifters that were located farther west in the Sargasso Sea on December 1, 2009, when the NAO wind anomaly began, also turned to the south and then southwestward, but their trajectories turned south farther offshore (west) of the African coastline than those described in the previous paragraph. They continued to move southwestward across the Atlantic in the NEC, eventually grounding on various Caribbean islands or otherwise ceasing to transmit within the Caribbean during 2011 and early 2012. This is the same period when the *Sargassum* inundations occurred there. For example, drifter 71,044 (dark green; Fig. 14) was deployed on October 10, 2008, and meandered in the Sargasso Sea until the start of the negative NAO event, during which it traveled along ~32°N from 35.8 to 19.4°W, covering a distance of 26.4 degrees of longitude in 121 days at an average speed of 0.15 m/s. It then turned to the southwest and eventually grounded on the northeast coast of the Dominican Republic a year later, on March 20, 2011.

During the NAO wind anomaly, a number of drifters were deployed within the Canary Current (colored drifters 71095, 90516, and 92023, and several more in gray). They all ended up grounding in the Gulf of Mexico/Florida Keys (71095, red), the Bahamas (90516, dark brown), and the eastern Caribbean (92023, yellow) during 2011.

The surface flow depicted by the drifters is generally to the south and southwest along the African coast north of about 16°N, then westward across the Atlantic in the NEC. Drifters deployed slightly farther south off West Africa generally turned to the east with the seasonally-developing NECC, and flowed east toward the Gulf of Guinea south of ~10°N. The distance that drifters traveled to the west from Africa in the tropical Atlantic (south of ~20°N) depended on the seasonal formation of the NBC retroflection and NECC. Some drifters reached as far west as 50°W (for example, 90522, shown in royal blue) before joining the eastward NECC (Fig. 14a). Upon reaching the coast of Africa some of the drifters turned back north along the African coastline circling counter-clockwise around the Guinea Dome. Others continued on to the east in the NECC and Guinea Current south of 10°N, where many eventually ran aground along the south coast of West Africa, east of 15°W. For example, drifters 92,024 (magenta) and 90,521 (light brown) grounded in 2011, just as the first *Sargassum* inundations were being reported for that area. Drifter 90,522 took longer to make its circuit of the NEC, NECC, and the Guinea Dome, grounding in the same area in early 2012.
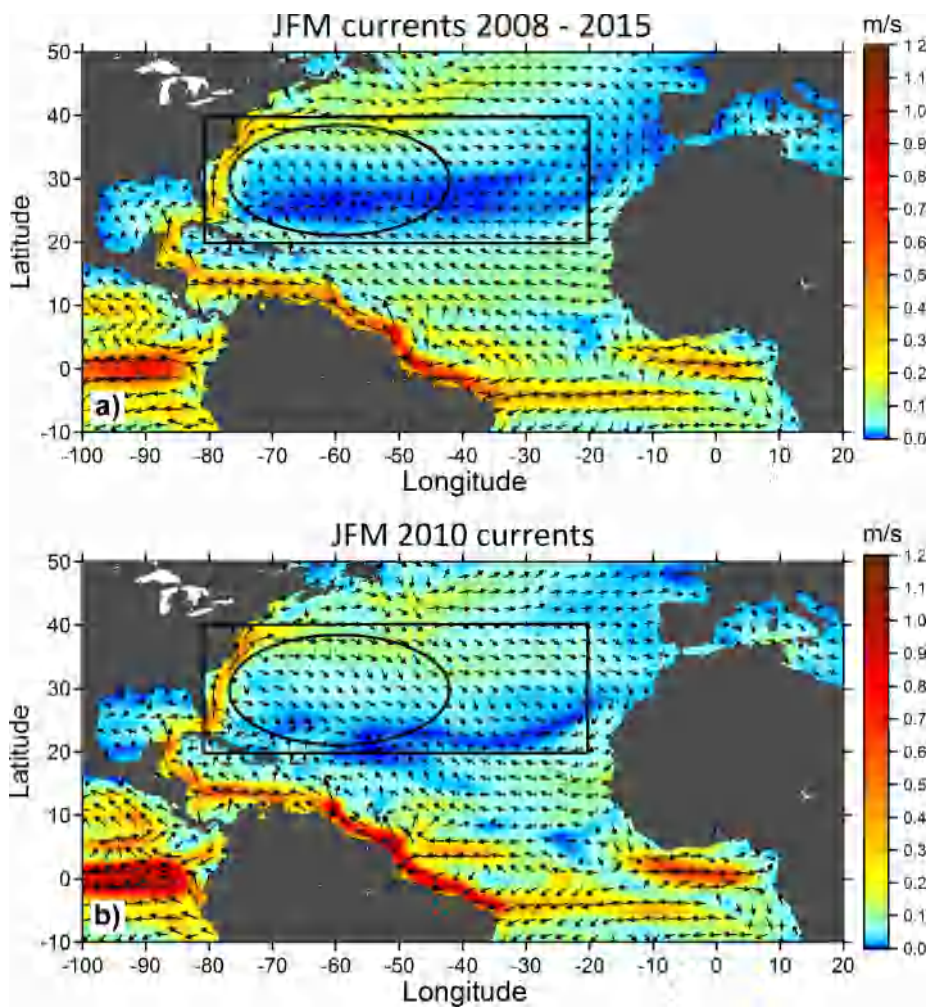
Fig. 7. (a) Climatological JFM surface currents for 2008–2015. (b) JFM 2010 surface ocean currents. In the climatological map the center of the subtropical gyre (dark blue tones, indicating the lowest velocities) is located at ~25–30°N in the Sargasso Sea, whereas it is shifted to the south during JFM 2010. Furthermore, the flow near Gibraltar which feeds the Canary Current originates in the 30–40°N latitude band in the Sargasso Sea during JFM 2010, whereas in the climatological map it comes from north of 40°N. The nominal Sargasso Sea is shown as a black oval, after Laffoley et al. (2011), and the black rectangle marks the 20–40°N, 80–10°W geographic box for the averaging shown in Fig. 9.

Direct connectivity between the Gulf of Guinea and northeast Brazil, where *Sargassum* was also first observed in 2011, is consistent with the trajectory of drifter 90,183 (violet). It crossed the Atlantic in the SEC at ~5°S, turned to the northwest, and stayed close to the coast of Brazil until ~5°N, 50°W. There it entered the NBC retroflection region until exiting to the northwest (perhaps tracking an NBC eddy) and eventually grounding in Guadeloupe on April 5, 2011. Two other drifters, 98,854 (medium green) and 75,247 (pale green) crossed the Atlantic from the eastern South Atlantic south of 10°S, and drifted to the northwest along the coast of Brazil towards the Caribbean Sea. Drifter 75,247 illustrates the complexity and intermingling of the tropical Atlantic currents as it turned east in the NBC retroflection and the NECC, but then crossed over into the westward flowing NEC and was finally transported into the central Caribbean where it stopped transmitting on May 1, 2011. Drifter 98854, on the other hand, remained very near to the coast until it stopped transmitting between Barbados and Grenada on September 27, 2011.

These drifter trajectories all support the hypothesis that between 30°N and 40°N *Sargassum* was advected far to the east between December 2009 and March 2010. Once the NAO wind anomaly ended, the drifters either moved southward, southwest and then westward in the NEC to the Caribbean Sea, or eastward toward the Gulf of Guinea in the NECC, areas where the 2011 *Sargassum* inundations were observed.

Fig. 14b shows the locations where the same selected drifters from Fig. 14a were deployed, where they lost their drogues, where they were located on June 1, 2010 approximately one year previous to grounding in the Caribbean, and where they grounded or otherwise ended their trajectories. The black dots show that the source regions for drifters that

ultimately grounded in the Caribbean in 2011 are to the north, along the coast of Africa in the Canary Current, and to the south, near the coasts of Africa and Brazil in the South Atlantic, in agreement with the results of the statistical drifter model (Figs. 12 and 13).

The green dots show where the drifters lost their drogues. In most cases the drogues were lost in the northern part of the domain and along the east side of the Atlantic, indicating that for much of their lifetimes, particularly during and after the NAO wind anomaly, these drifters were undrogued and would have moved similarly to other partially submerged objects subject to 1% windage as previous studies have shown (Lumpkin and Pazos, 2007; Lumpkin et al., 2013).

The locations of the drifters on June 1, 2010, two months after the NAO wind anomaly ended, are shown as red dots in Fig. 14b. For those drifters that ended up in the Caribbean, the Bahamas, or the Gulf of Mexico in 2011, these red dots show where they came from roughly one year prior. Most of the drifters that entered the Caribbean Sea were located far from the Caribbean on June 1, 2010, along the coast of Africa (at ~2°N, 0°W), in the South Atlantic (~6°S, 17°W), along the coast of northeast Brazil, and in the northeast Atlantic, illustrating the range of possible one-year prior sources and the timing that it takes to move from those areas to the Caribbean.

Most of the drifter groundings (blue dots) occurred in the Caribbean Sea, the Bahamas, the Gulf of Mexico, and the Florida Keys during 2011 and early 2012, coincident with the observed dispersal and beaching patterns of *Sargassum*. Some of the drifters ran aground on the coasts of Morocco (~28°N, 13°W) during April-July 2010, and Ghana (~4°N, 2°W) during March of both 2011 and 2012 (Fig. 14b). This coincided with coastal *Sargassum* inundations reported there (UNEP, 2015).
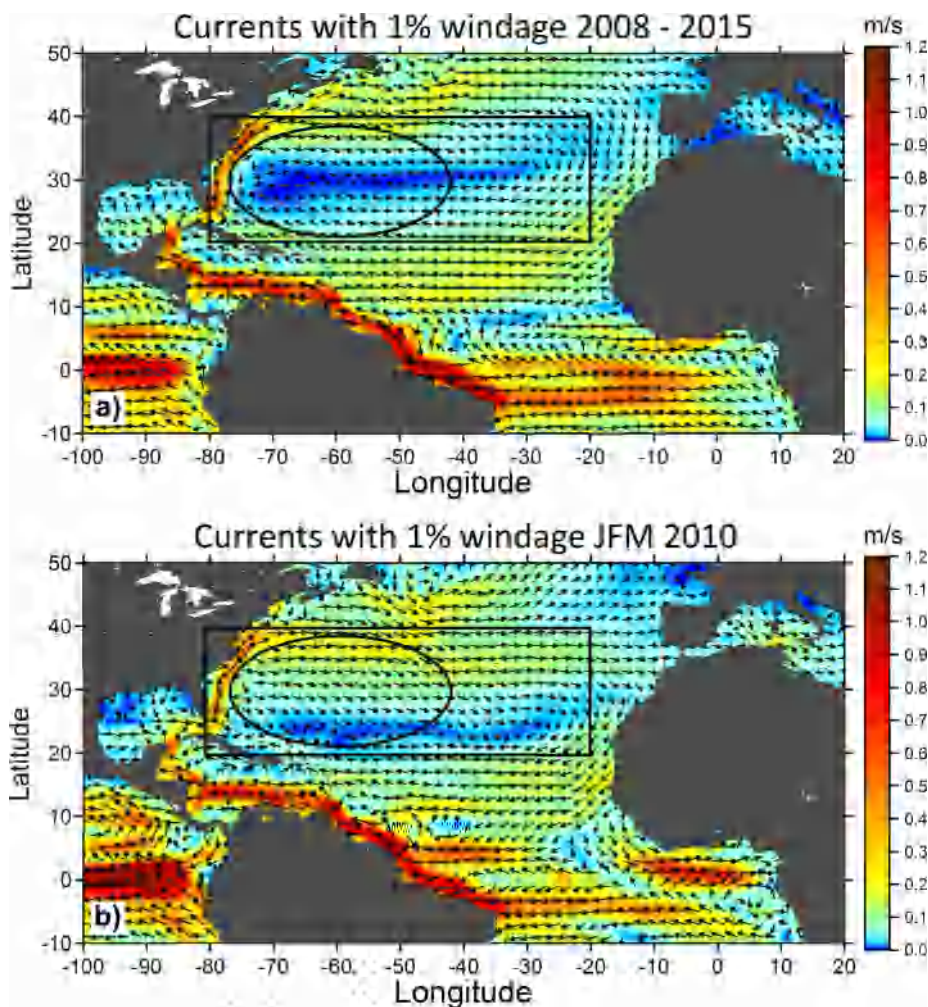
Fig. 8. (a) Climatological JFM surface ocean currents including 1% windage for 2008–2015. (b) Surface ocean currents for including 1% windage for JFM 2010. The currents with windage are generally stronger and better organized. In the region of just west of Gibraltar, the difference between the climatological currents and the JFM 2010 currents is accentuated. The nominal Sargasso Sea is shown as a black oval, after Laffoley et al. (2011), and the black rectangle marks the 20–40°N, 80–10°W geographic box for the averaging shown in Fig. 9.

4.4. Time series observations of in situ Sargassum

Net tow observations of *Sargassum* were obtained by the Sea Education Association (specifically during the cruises listed in the references as Sea Education Association (2006–2016). We used only a subset of the total dataset (2006–2016) for the present analysis. Net tow stations and the geographic boxes used in the analysis are shown in Fig. 15a. Time series of the *Sargassum* data are shown in Fig. 15b and c. Data from the Slope Water box (off northeast North America) are not shown, as there was no *Sargassum* observed in the slope water between 2006 and 2016. No data are shown for the Gulf of Mexico either, due to insufficient data quantity and spatial coverage there.

Prior to 2011, *Sargassum* abundances were small (≪ 500 g/tow) in the eastern and western Caribbean regions (Fig. 15a, blue and red, respectively). Values in the Caribbean began to rise in spring 2011, reaching over 1000 g/tow by late 2011, and nearly 4600 g/tow in April 2012, before falling abruptly to near-zero by the beginning of 2013. The absence of a *Sargassum* bloom during 2013 was also noted for the tropical Atlantic inundations in the Caribbean during 2013 using satellite imagery (Wang et al., 2019a and Fig. 1d). *Sargassum* returned to the eastern Caribbean in 2015 and 2016, but in much smaller amounts.

In the tropical Atlantic, prior to 2011, there was virtually no *Sargassum* in the net tows (Fig. 15b, green), but it started to appear in 2011 and peaked in 2012, at the same time as the peaks in the eastern

and western Caribbean. *Sargassum* abundance was minimal in 2013 and early 2014, but at the end of 2014 there was a large peak, and values were high also in late 2015.

The interannual variation in net tow collections in the Sargasso Sea (Fig. 15c, gold) suggests that the large-scale movement of *Sargassum* out of the Sargasso Sea and into the tropics may be reflected in a decrease in *Sargassum* concentrations in the Sargasso Sea immediately after the winter 2009–2010 NAO wind event. Following the NAO wind event in December 2009 through March 2010, values indeed dropped until late 2011 (Fig. 15c). Subsequently, the *Sargassum* rebounded. Following the March 2013 strongly negative NAO (Fig. 3b) and accompanying strong anomalous eastward winds, the levels of *Sargassum* in the Sargasso Sea again returned to near-zero and remained low through at least early 2016.

4.5. Time series of remotely-sensed Sargassum

We conducted several analyses using both the MERIS and MODIS satellite data to better understand the timing of the dispersal of *Sargassum* out of the Sargasso Sea, its range expansion to the tropical Atlantic, and the tropical Atlantic blooms that have occurred nearly every year since 2011. These are described below.
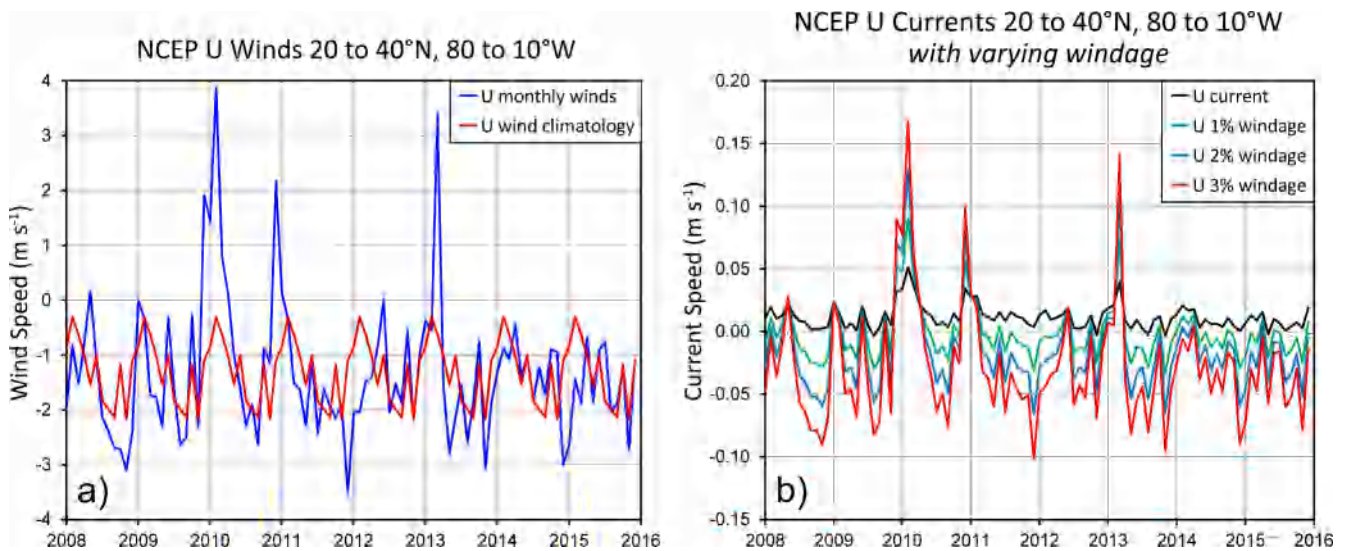
Fig. 9. (a) Time series of the monthly NCEP wind climatology (red) and the monthly NCEP winds (blue) averaged over 20–40°N, 80–10°W (the black rectangle shown in Figs. 7 and 8). The climatological winds in the 20–40°N band are weak and to the west, whereas in the three strongly negative NAO events (December 2009 through March 2010, December 2010, and March 2013) the direction is reversed and the winds are strong and to the east. (b) NCEP zonal surface ocean currents within the 20–40°N, 80–10°W box, with windage of 1, 2, and 3% applied. The average currents with no windage (black) are low and to the east for the non-anomalous time periods, whereas the currents with windage (green, blue, and red as in the Key) are generally directed towards the west. During the three NAO anomaly periods, the currents with no windage and with the varying windage percentages are all strong and directed to the east with varying magnitudes according to the windage percentages.
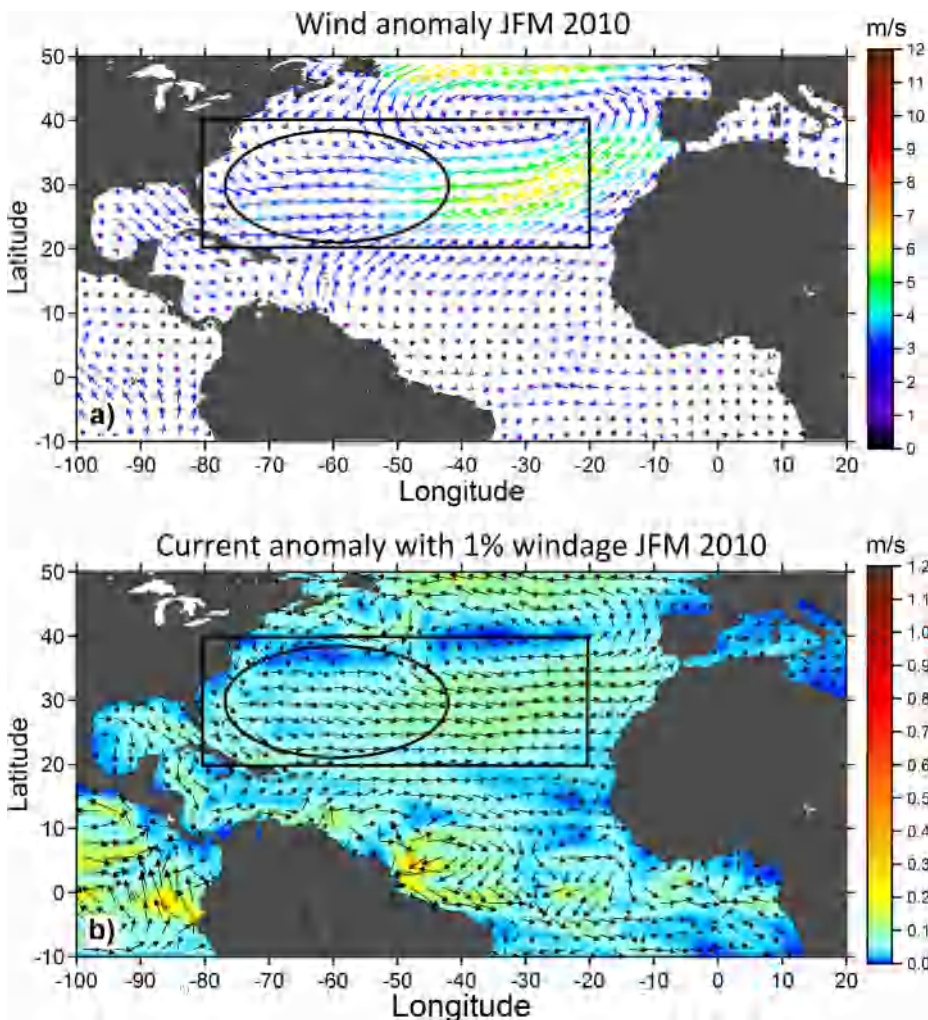
Fig. 10. The anomalies of the *u* and *v* components of the velocity were calculated by subtracting the climatological values from the JFM 2010 values at each grid point. These anomalies were then plotted as a vector map with the direction shown by the arrows, and the magnitude shown by both the arrow length and the contoured colors. The NAO wind anomaly primarily affects only the northern part of the mapped domain, with the dominant feature being the strengthened westerlies and their shift to the south. The ocean currents show a similar feature north of 20°N. (a) Anomaly of the winds during JFM 2010. (b) Anomaly of the surface ocean currents with 1% windage during JFM 2010.
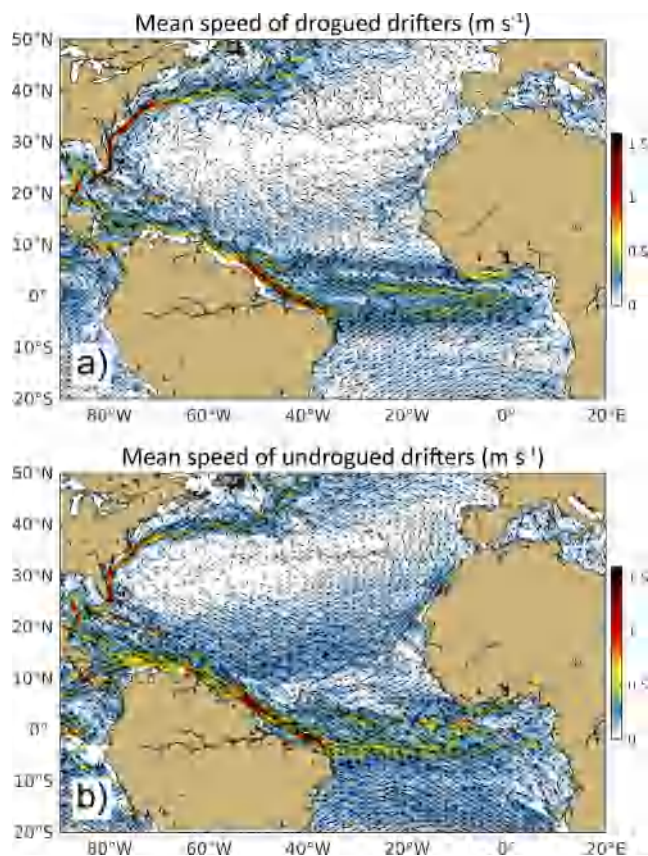
Fig. 11. (a) Climatological circulation patterns in the North Atlantic based on drogued drifter data. (b) Climatological circulation patterns in the North Atlantic based on undrogued drifter data. Data were averaged over the period 1979 through July 2018. The average current speeds from the undrogued drifters are generally stronger than those obtained using only drogued drifters, and show striking changes in the locations and directionality of some of the currents, particularly a strengthening of the subtropical gyres in the North and South Atlantic. The southward flow near Gibraltar and in the Canary Current is also stronger and more organized in the undrogued drifter map.

4.5.1. Timing of the arrival of the new Sargassum population in the tropical Atlantic

Fig. 1a shows geographical boxes used for averaging the MERIS satellite sensor Maximum Chlorophyll Index (MCI; Gower et al., 2006; Gower and King, 2008; Brooks et al., 2018). Fig. 1b shows the MCI averaged in a band between 10 and 20°N in the eastern Caribbean Sea (66–60°W) and two areas of the western tropical Atlantic (60–50°W and 50–40°W). The index shows low to undetectable *Sargassum* abundances until early 2011 in the Caribbean Sea and the western tropical Atlantic. Fig. 1c shows results 10 degrees farther south between latitudes 0–10°N, for the longitudes 60–50°W (western tropical Atlantic), and eastward to 50–40°W, 40–30°W, 30–20°W, and 20–13°W up to the West Africa coast. The MCI increased first in 2010 in the three subregions of the western tropical Atlantic to the southeast of the Caribbean (Fig. 1c). This was followed by the *Sargassum* abundance peak in the eastern Caribbean in 2011.

The MERIS sensor ceased to function in 2012. The observations of Wang and Hu (2017, 2018) and Wang et al. (2019a, 2019b) using the MODIS sensor extend the time series of *Sargassum* area cover through 2018 (Fig. 1d). Wang et al. (2019a) confirm the low *Sargassum* densities in the tropical Atlantic prior to 2011. Large blooms occurred typically in April-July of 2012, 2014, 2015, 2016, 2017, and 2018. The satellite data also showed low *Sargassum* densities during all of 2013, early 2014 and early 2016.
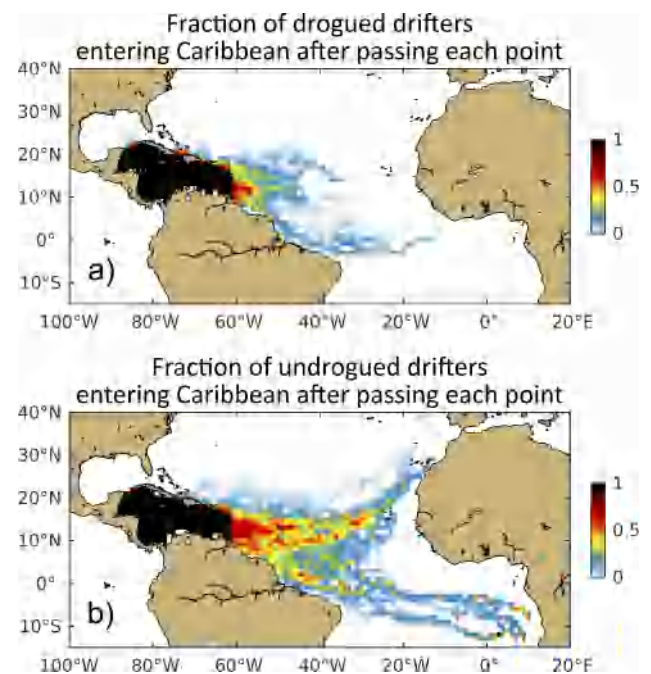

Fig. 12. Maps showing the fraction of drogued vs undrogued drifters passing through each 1 × 1° bin that subsequently end up in the Caribbean (black bins). Data are from the period 1979 through March 2018. (a) Drogued drifters have a limited set of paths from the east, and the main pathway connects to the South Atlantic. (b) Undrogued drifters, in addition to having a stronger and more extensive connection to the South Atlantic, also have a clear connection linking the eastern tropical and subtropical Atlantic and Canary Current region with the Caribbean.

4.5.2. Seasonal aggregation of the Sargassum in the tropical Atlantic – A giant windrow under the ITCZ

In this section, we consider mechanisms that can aggregate floating material along a zonal band in the tropical Atlantic and possible nutrient sources to sustain these yearly blooms. We re-examine MODIS-derived time series of *Sargassum* densities and spatial distribution patterns from Wang et al. (2019a, 2019b) in the context of the seasonal migration of the ITCZ, the seasonal surface circulation in the central tropical Atlantic, wind-induced Ekman pumping, changes in the mixed layer depth (MLD) in the tropical Atlantic, and nitrate availability at the surface and within the MLD.

Fig. 16 shows the average (2010–2018) seasonal cycles of the lower atmosphere wind divergence over the tropics, the ITCZ in the maximum of wind convergence (negative divergence), and surface ocean currents, in relation to *Sargassum* coverage > 0.02% based on MODIS data. From April through September, the windage exerted by the wind convergence accumulates the *Sargassum* within the ITCZ. Between May-June the *Sargassum* is accumulated by the wind convergence in the western region of the ITCZ, until the NBC retroflects joining the NECC. From July to October, the NECC helps redistribute the *Sargassum* eastward, extending the *Sargassum* windrows across the Atlantic all the way to West Africa.

Fig. 17 shows the monthly averages (2010–2018) of *Sargassum* density based on MODIS data from Wang et al. (2019a, 2019b), along with the averages of the ITCZ position, the open-ocean upwelling due to the wind stress curl (positive Ekman pumping), and the chlorophyll > 0.2 mg m^{-3}. Positive Ekman pumping occurs in the middle of the Atlantic Ocean between June and October with an offset to the north of the ITCZ, coinciding with the accumulation of *Sargassum* along the ITCZ.

Sargassum patches start aggregating in the region of convergence of the trade winds (i.e., the ITCZ) between about March and April (Fig. 17). From May to September, *Sargassum* is "tightly packed" in a
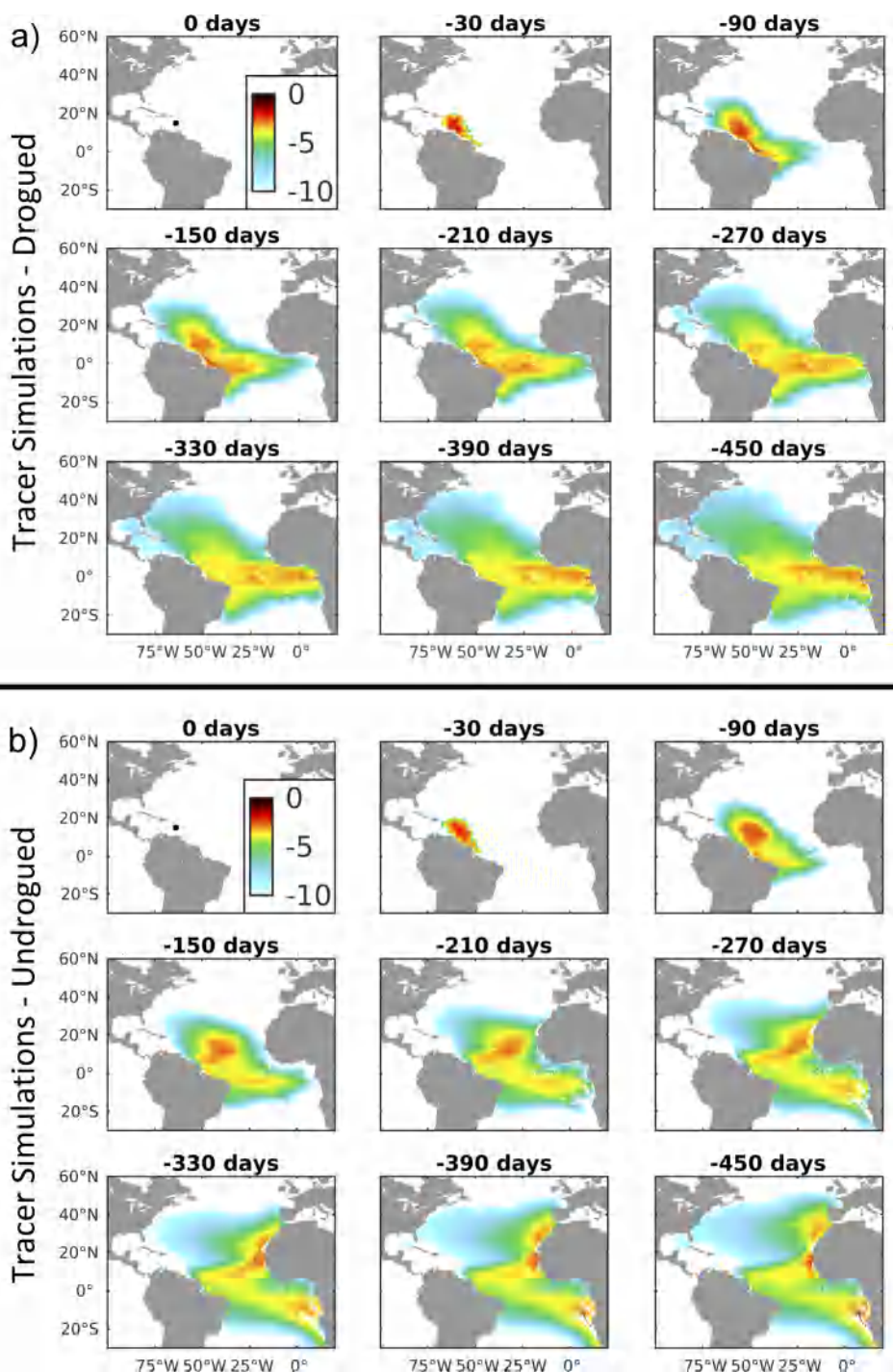
Fig. 13. Tracer simulations based on observed drifter statistics, backtracked from a starting point in the eastern Caribbean Sea (shown as the black dot in the "0 days" maps). The colors are log 10 (concentration), where the starting concentration is 1 (arbitrary units), and the time step is every 60 days after the 30 day maps, up to 450 days. (a) Tracer simulations using drogued drifter statistics. (b) Tracer simulations using undrogued drifter statistics.

giant windrow along the ITCZ. The NECC contributes to the eastward transport of *Sargassum* (Fig. 16). This windrow moves north following the ITCZ in its seasonal migration. In October, when the wind convergence weakens and the ITCZ starts its southward migration, the *Sargassum* belt is left behind in the subtropical North Atlantic (large red ovals in Fig. 17).

The monthly average chlorophyll concentration in Fig. 17 also shows the typical position and extent of the Amazon and Orinoco River plumes, and of the upwelling plumes off northwest Africa and the equator, in relation to the seasonal *Sargassum* accumulation in the

tropical Atlantic. Between March and May, the *Sargassum* accumulation area can be located several degrees of latitude to the south of the area of northwestward extension of the Amazon plume. In July and August, *Sargassum* can be found in the area of the Amazon plume, and by September and October, it can also be found east of the Amazon plume. The trans-Atlantic *Sargassum* windrow forms south of the northwest Africa upwelling region and north of the equatorial upwelling. The upwelling along the equator typically has maxima between June and September (Weisberg and Tang, 1985, 1990; Weisberg and Colin, 1986; Weingartner and Weisberg, 1991; Carton and Zhou, 1997; Grodsky
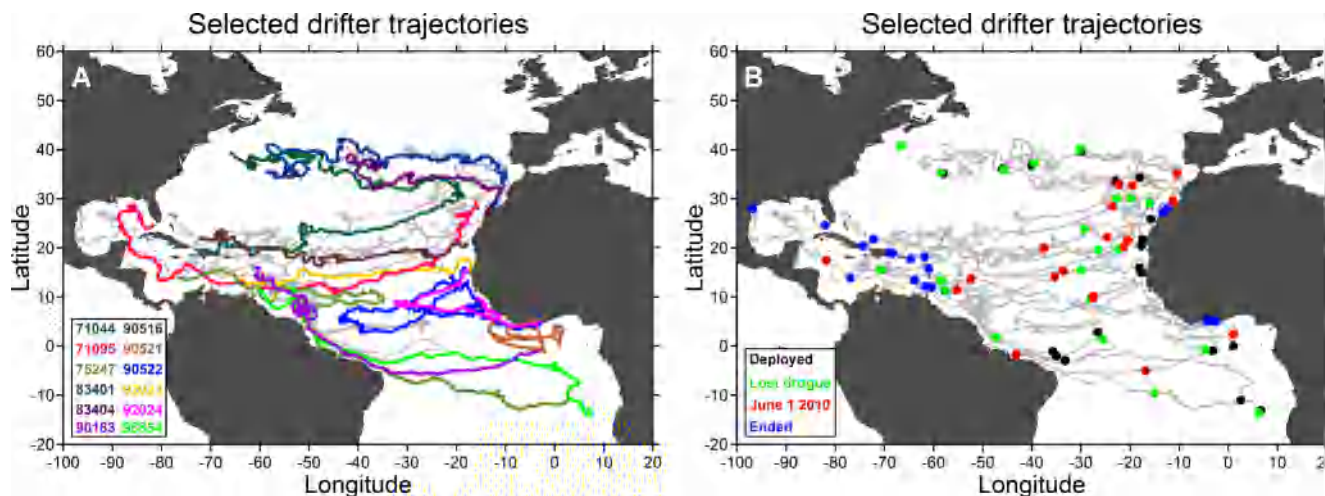
Fig. 14. (a) Individual drifter trajectories from the NOAA Global Drifter Program illustrate the range of possible pathways from the Sargasso Sea to grounding in the various areas where the *Sargassum* inundations occurred in 2011. (b) The same drifters shown in (a) are all shown in gray. Filled colored circles indicate the locations where these drifters were deployed (black), lost their drogues (green), were located on June 1, 2010 (red) approximately one year prior to entering the Caribbean Sea, and ended mostly due to grounding (blue).
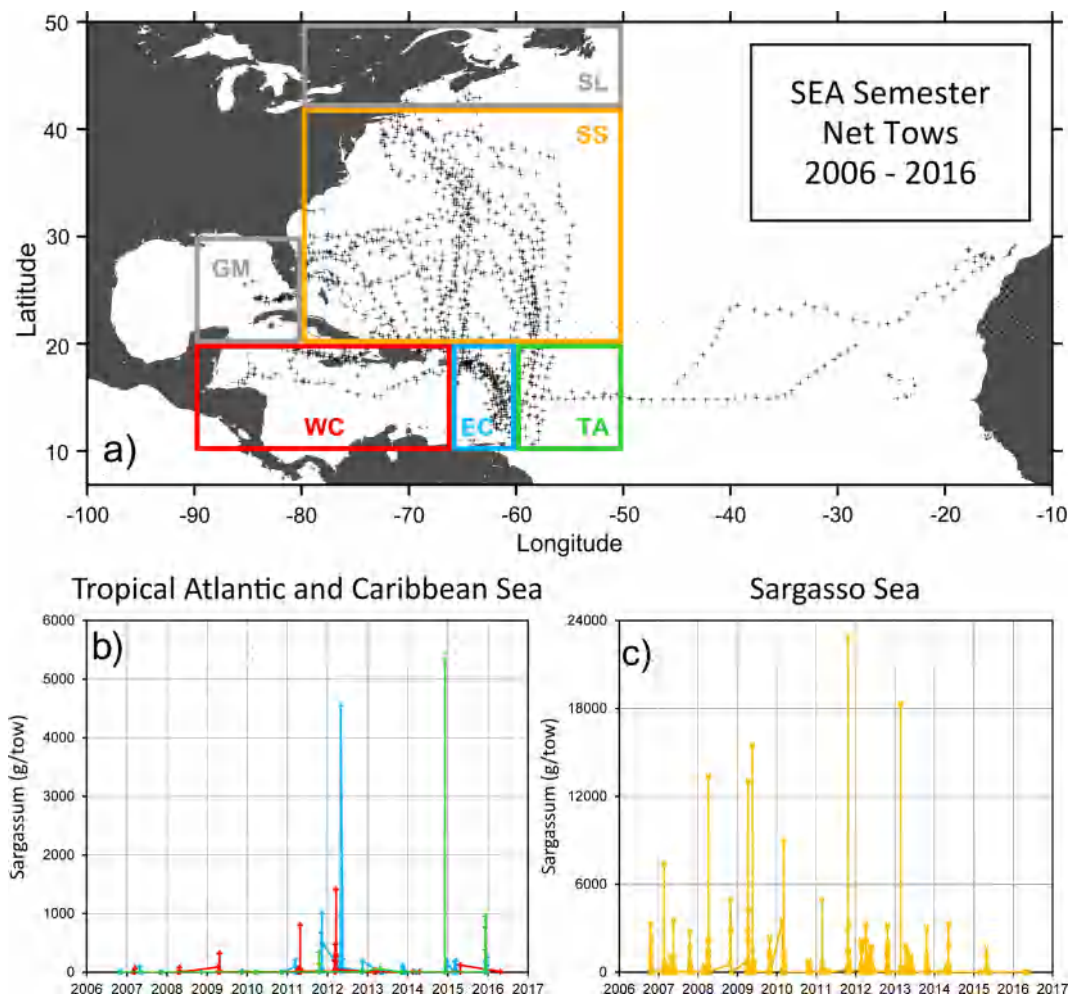
Fig. 15. (a) Locations of SEA Semester net tows for *Sargassum* biomass collected between 2006 and 2016. SS denotes the Sargasso Sea, EC is the eastern Caribbean, WC is the western Caribbean, and TA denotes the tropical Atlantic. The SL (slope water) and GM (Gulf of Mexico) boxes were not used in the analysis. (b) *Sargassum* biomass (defined as S. *natans I + S. fluitans III*) in units of grams per 1 km net tow in the eastern Caribbean (blue), western Caribbean (red), and the tropical Atlantic (green) regions. The ship sampled only limited time periods and thus does not capture events such as the 2015 high *Sargassum* density in the Caribbean Sea. The ship data are valuable to examine biomass and taxonomy of the *Sargassum* in tandem with the satellite-based time-series observations (e.g., Fig. 1). (c) *Sargassum* biomass (defined as S. *natans I + S. fluitans III*) in units of grams per 1 km net tow in the Sargasso Sea region. Note the change of y-axis scale from 0 to 6000 g/tow for the Caribbean and tropical Atlantic to 0 to 25,000 g/tow for the Sargasso Sea.
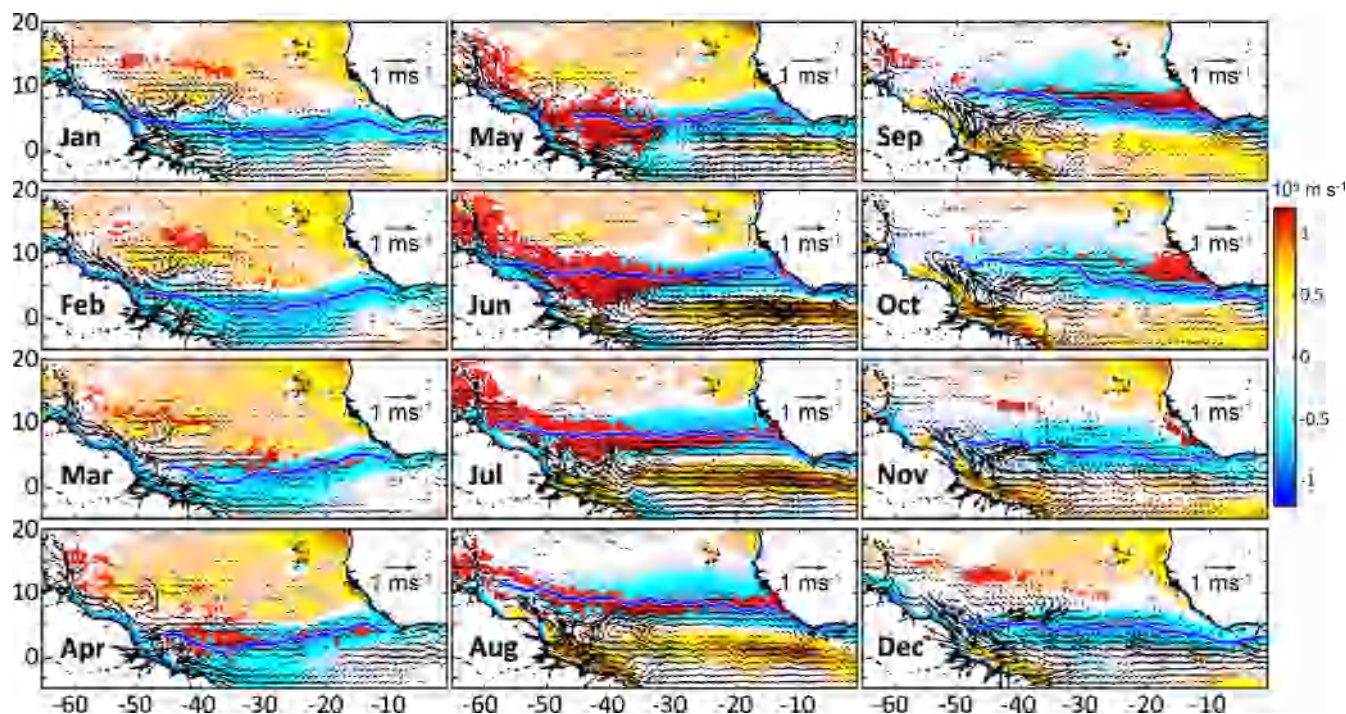
Fig. 16. Monthly long-term averages (2010–2018) of wind divergence (colored contours), showing the location of the ITCZ (the maximum of wind convergence or negative divergence, with the ITCZ's position illustrated as a bold blue line); near-surface currents are shown as vectors (the arrow shown over Africa represents the scale for $1 \, \text{m s}^{-1}$; for clarity, only currents $\geq 0.1 \, \text{m s}^{-1}$ are displayed); and monthly average of percentage of *Sargassum* coverage ($> 0.02\%$, red circles). The *Sargassum* is seasonally concentrated within areas of wind convergence between April and September. Around May, the NECC forms, and the NBC retroflects joining the NECC. From June to September the NECC helps to spread the *Sargassum* aggregation across the Atlantic along the ITCZ. Atlantic wind divergence calculated from satellite wind CCMP product, ocean currents from OSCAR (Ocean Surface Current Analysis Real-time), *Sargassum* density adapted from Wang et al. (2019a, 2019b).

et al., 2008). But at this time, the *Sargassum* accumulation is already 7–10° farther to the north of the equatorial upwelling (Fig. 17).

We evaluated the mixed layer and nutrient conditions under the *Sargassum* belt in the tropical Atlantic (Fig. 18). We focused on the MLD and nitrate concentration observations only in the areas where *Sargassum* coverage averaged $> 0.001\%$ within the area 0-15°N and 15-55°W (see Fig. 1a). The anomalies in *Sargassum* coverage show a direct relationship with the anomalies in the deseasonalized MLD time series (Fig. 18a). Higher correlations were observed with a lag of one and two months of MLD leading changes of *Sargassum* (1-month $r = 0.54$, $R^2 = 0.29$, $p < 0.001$, $n = 107$; 2-months $r = 0.56$, $R^2 = 0.31$, $p < 0.001$, $n = 106$). The MLD anomalies were related to anomalies of the ocean surface turbulence due to the wind stress (calculated as the square of the 6-hours wind speed, $r = 0.71$, $R^2 = 0.50$, $p < 0.001$, $n = 108$). The seasonal variability of the MLD under the *Sargassum* belt tends to be deeper than or similar to the nitrate nutricline (calculated as the depth where nitrate concentration increased by $\geq 0.5 \, \mu\text{M}$ relative to the surface; Fig. 18b). Nitrate averaged within the MLD was usually higher than the nitrate concentration averaged over the first 10 m of the surface (Fig. 18c). These analyses show that the MLD can be deep enough so that nutrients are available to the large accumulation of the *Sargassum* in the equatorial Atlantic.

Our results show that *Sargassum* accumulates under the ITCZ and is stretched eastward along the ITCZ by the NECC. We also show that in the tropical Atlantic, *Sargassum* has diverse nutrient inputs, such as upward nutrient flux driven by eddy diffusion (e.g., McGillicuddy et al., 2003), upward entrainment of nutrients as the mixed layer deepens seasonally, seasonal contact with the Amazon River plume, and also positive Ekman pumping (open-ocean upwelling) due to the curl of the wind (Fig. 17).

5. Discussion

5.1. Expansion of the biogeographical range of Sargassum

Six lines of evidence were described in the Methods and Results sections above, namely (1) numerical circulation models, (2) wind and current reanalysis data, (3) drogued and undrogued drifting buoys, (4) *Sargassum* data from *in situ* net tows, (5) satellite ocean color data, and (6) historical hydrographic observations. Their joint analysis supports the conclusion that, triggered by an extreme wind anomaly during the record-breaking negative NAO of December 2009 through March 2010, and including a 1% windage, there was a redistribution of *Sargassum* from the Sargasso Sea to the tropical Atlantic. We suggest that this population is the cause for the now recurring large blooms in the central tropical Atlantic and for the blooms that affect coastal areas of Africa, the Caribbean, and the Gulf of Mexico. As of mid-2019, the coastal *Sargassum* inundations continue to negatively affect these areas.[2]

After being exported to the tropical Atlantic from the Sargasso Sea, populations of these *Sargassum* species are now recirculating between the western and eastern tropical Atlantic, in the seasonally-varying NEC, NECC, and SEC, and aggregating along the ITCZ. From there, they are exported seasonally to the Caribbean Sea and beyond by the ocean currents of the tropical Atlantic (Putman et al., 2018). Subsequent to the "*Sargassum* events" of 2011, there have been unprecedented accumulations of mixed *S. fluitans* and *S. natans* species reported in 2014 to 2016 off the coast of San Andres island in the southwestern Caribbean (Gavio et al., 2015), in the Ivory Coast area of West Africa (Komoe et al., 2016), in Punta Cana on the eastern shore of the Dominican Republic (Baez et al., 2016), and off northeast Brazil (Sissini et al.,

---

[2] https://www.theatlantic.com/science/archive/2019/07/great-atlantic-sargassum-belt-here-stay/593290/.
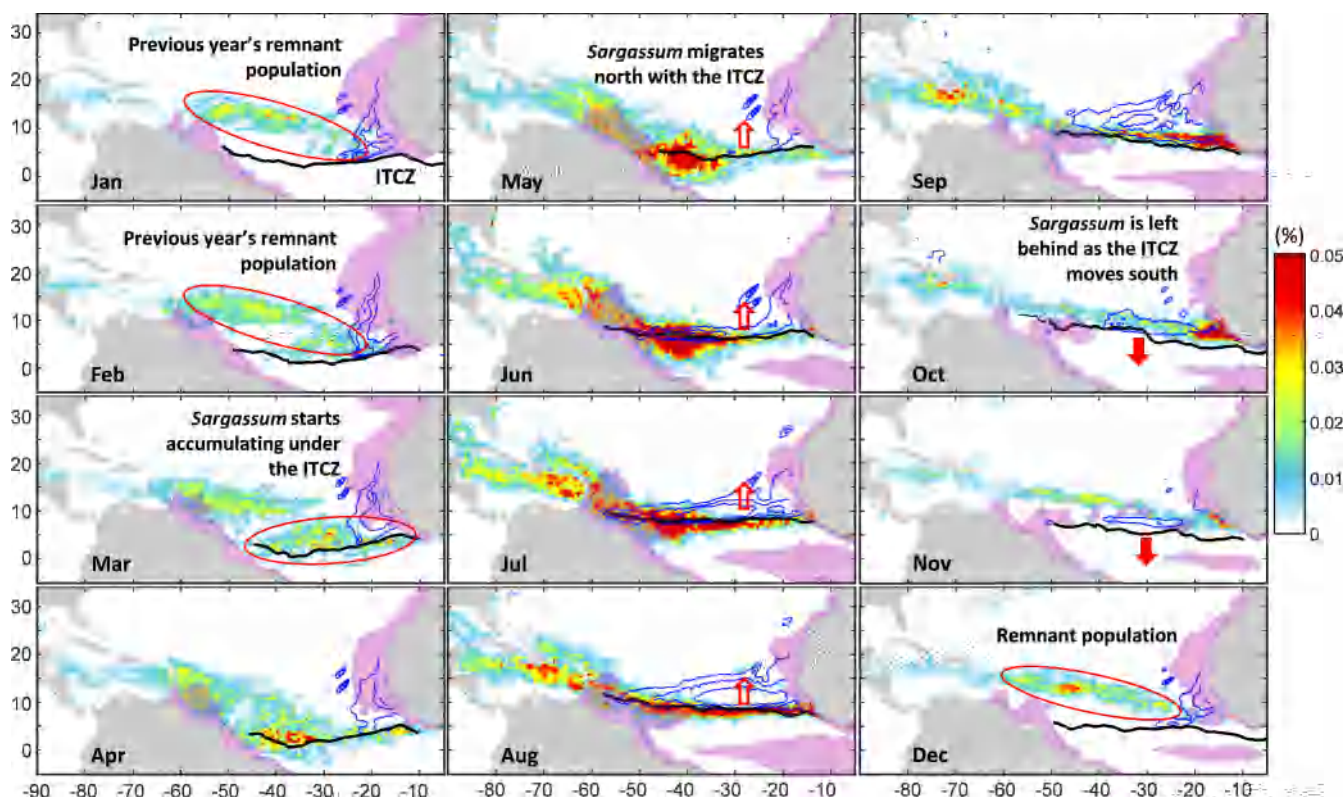
Fig. 17. Monthly averages (2010–2018) of: *Sargassum* density (color bar shows % spatial coverage). The Inter-Tropical Convergence Zone (ITCZ) climatological position is indicated here with a black line tracing the broad area of maximum in wind convergence show in Fig. 16. Ekman pumping is shown by the blue isolines for 0.1, 0.2, and 0.3 m d^{-1} (increasing thickness of the contours indicates progressively larger Ekman pumping). The areas where the average Ekman pumping was > 0.1 m d^{-1} are areas of open-ocean upwelling. Open-ocean upwelling occurs over a large area to the north of the ITCZ from June until October, when *Sargassum* accumulates along the ITCZ. During May-September, *Sargassum* accumulates in the central tropical Atlantic due to wind convergence (see Fig. 16). The trans-Atlantic *Sargassum* wind row then follows the ITCZ in its seasonal northward excursion (red open arrows). Starting in October, when the wind convergence weakens (see Fig. 16) and the ITCZ starts its southward excursion (filled red arrows), *Sargassum* patches are left behind. In December-March, remnant *Sargassum* patches are still observed around 10°N (red ovals). As the ITCZ starts to migrate north again in its following annual cycle, remnant *Sargassum* patches aggregate due to the wind convergence. The purple filled-in areas show regions of satellite-derived apparent chlorophyll concentrations > 0.2 mg m^{-3}. These show the location of the plumes of the Amazon River, Orinoco River, and phytoplankton blooms in the western and eastern Atlantic. They also illustrate the extent of the northwest Africa upwelling plume. In the equatorial region, the purple areas trace the phytoplankton bloom caused by seasonal upwelling. Atlantic wind divergence, ITCZ, and Ekman pumping calculated from the satellite wind CCMP product (Ekman pumping within 200 km of continents, around the equator, and outside the north tropic was masked). *Sargassum* density derived using MODIS satellite data adapted from Wang et al. (2019a, 2019b). Purple contours were traced by hand from the monthly climatology (2002–2018) of the NASA MODIS chlorophyll concentration product derived from ocean color (source: Goddard Space Flight Center).

2017) which are indicative of a Sargasso Sea origin, although they were not identified to the sub-species level in these particular studies.

It should be noted that Schell et al. (2015) found that a formerly rare sub-species of *Sargassum* (*S. natans VIII*) was dominant in the western tropical Atlantic and eastern Caribbean in late 2014 to early 2015. This observation suggested that the origin of the *Sargassum* accumulations found in these regions was not the Sargasso Sea. However, there are recent indications near the northern Caribbean and passages of the Greater Antilles of a shift back from the previously dominant *Sargassum natans VIII* morphotype, with all three morphological forms of pelagic *Sargassum* now present (*S. fluitans III* and *S. natans I* and *VIII*; J. M. Schell, personal communication, 2019), suggesting a return to the higher influxes of *Sargassum* from the Sargasso Sea.

It remains to be seen whether this new expanded range of pelagic *Sargassum* can be maintained over time despite the dispersive effects of the prevailing winds and surface currents in the tropical Atlantic, effectively establishing a new "tropical Sargasso Sea".

5.2. Formation and seasonal migration of the tropical Atlantic Sargassum bloom

The sequence of annual satellite-derived maps of the ITCZ and of the *Sargassum* bloom from 2010 to 2018 clearly show that the *Sargassum*

concentrates under the ITCZ (Figs. 16 and 17). In effect, the surface wind convergence aggregates *Sargassum* into a broad trans-Atlantic windrow along the ITCZ. As the Earth's northern hemisphere is progressively exposed to the sun in the transition from northern winter to summer, the ITCZ shifts northward roughly at a speed of 5 km d^{-1}, moving the *Sargassum* windrow with it. The time series of ocean currents, wind convergence, and *Sargassum* density suggests that as the *Sargassum* windrow moves through the region where the seasonal NECC forms (June-July), the eastward current helps it to spread to the eastern tropical Atlantic. At this time, the *Sargassum* benefits from nutrients from the open-ocean upwelling due to the wind curl, as well as from nutrients from the Amazon plume, which is advected east around the NBC retroflection into the NECC (Muller-Karger et al., 1988, 1995; Hu et al., 2004). In August, the bulk of the *Sargassum* aggregation is transported northward with the ITCZ past the latitude of the NECC and the Amazon River plume. Some of this *Sargassum* is also entrained in the northwestward drift of the NEC/NBC/GC system that enters the Caribbean Sea (Figs. 2 and 17). Eddy entrainment likely enhances this transport pathway (Brooks et al., 2019).

As the ITCZ reaches its annual northernmost position in about September, the converging winds weaken (Fig. 16), and the ITCZ initiates its southward excursion, leaving the *Sargassum* row behind (Fig. 17). The trade winds and the NEC, however, maintain this
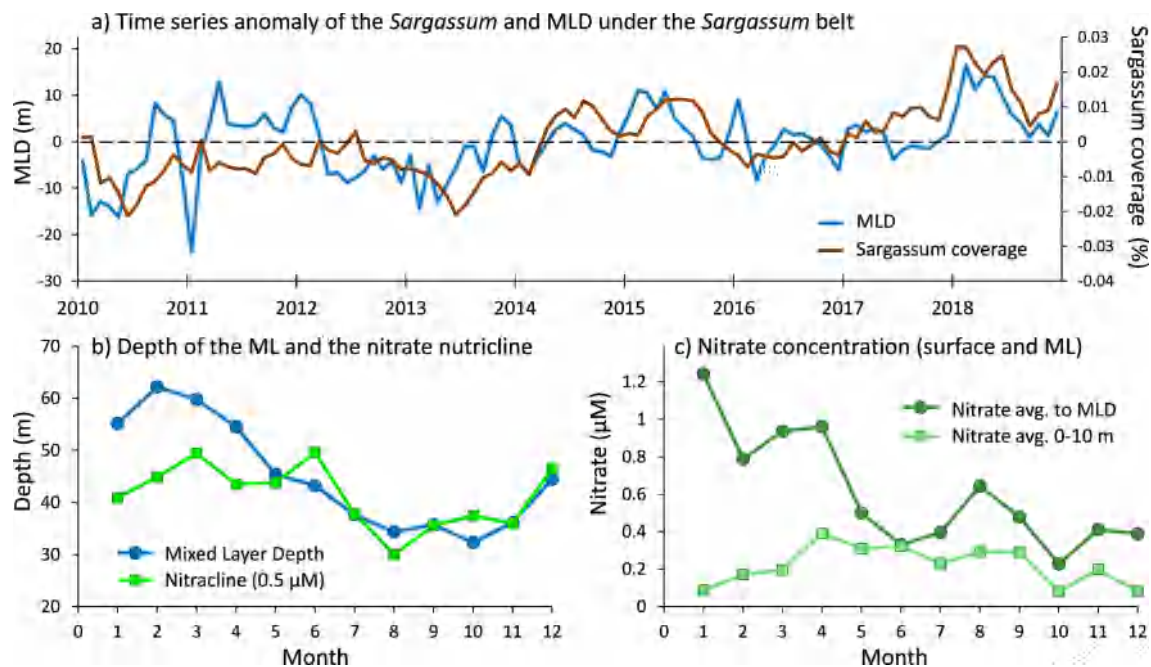
Fig. 18. Mixed Layer Depth (MLD) and nitrate under the *Sargassum* belt in the Tropical Atlantic. Data were extracted every degree within 0–15°N and 15–55°W (see green and blue boxes in Fig. 1a); spatial averages were calculated only for the one-degree locations with *Sargassum* density > 0.001%. (a) Monthly anomaly time series (minus the seasonal signal) of the MLD and monthly anomaly time series of the *Sargassum* spatial coverage (minus the seasonal signal). Higher positive MLD anomalies indicate deeper MLD compared with the climatology. (b) Long-term monthly averages of the MLD (2010–2018) and the nutricline (calculated as the first depth where nitrate ≥ 0.5 μM/kg). (c) Long-term monthly nitrate averages for the surface (0–10 m depth) and within the mixed layer. *Sargassum* density as per Wang et al. (2019a, 2019b); MLD obtained from the ECCO2 model; nitrate climatology from the NOAA World Ocean Atlas 2018 (WOA2018 objectively analyzed mean).

northward position of the *Sargassum* row as they advect it to the west toward the Caribbean as described by Putman et al. (2018). Under this scenario, the remnant patches of *Sargassum* left behind by the ITCZ serve as the seed population for a new accumulation the following year (Fig. 17). The patches in the vicinity of the Guinea Dome increase in density during December-January, when upwelling there is strong. The subsequent aggregation of *Sargassum* into another large windrow across the entire Atlantic under the ITCZ by March gives a visual impression of either extremely fast advection or of fast growth. We suggest that the increase in biomass is mainly due to physical aggregation along the ITCZ by the wind convergence.

Wang et al. (2019a; see their Supplemental Materials) argue that the Amazon River is an important contributor to the formation of the Atlantic *Sargassum* aggregation. They offer as evidence a comparison of nutrient data collected during cruises in May-June 2010, and in May-June 2018. Wang et al. (2019a) found very low to undetectable inorganic nutrient values in offshore plume waters in 2010, compared to much higher nutrients (nitrogen > 1 μM) in 2018, and attributed the higher values in 2018 to human activities upstream in the Amazon River basin, including deforestation, agriculture, and other development. However, their samples were collected in an area northwest of the Amazon River's mouth (i.e., west of 50°W), not offshore in the central tropical Atlantic where the *Sargassum* is concentrated. Muller-Karger et al. (1995) examined historical reports of significant export of nutrients in the Amazon plume. Vigorous recycling as well as upwelling is associated with the NBC retroflection, and NBC rings can also lead to high surface nutrient levels (e.g., > 1 μM in inorganic nitrogen) at distances exceeding hundreds of km from the Amazon River mouth. The higher nutrients found during 2018 by Wang et al. (2019a) are not a new occurrence for this region. Indeed, based on the historical observations, the lower nutrient values reported by Wang et al. (2019a) for 2010 are the anomaly. This anomaly is consistent with the higher current speeds and other circulation anomalies observed in the region during the negative NAO event of 2010 (Figs. 8 and 10).

The Amazon plume dispersal patterns also do not coincide with the

spatial location of formation of the *Sargassum* windrow in the tropical Atlantic in March-May (Fig. 17). When the windrow forms, along ~2°N and under the ITCZ, the NBC and GC are carrying Amazon River waters to the northwest of the Guianas at high speeds. The Amazon River water is advected into a region that is largely contained north of 5°N and west of 50°W (Muller-Karger et al., 1988, 1995; Hu et al., 2004). As such, the *Sargassum* aggregation probably benefits most from Amazon River nutrients after June, when it crosses the latitude of the NECC. Once the *Sargassum* has reached the Caribbean, it likely benefits from additional nutrients provided by the Orinoco River plume as well (Johns et al., 2014).

We also examined the historical position and extent of the upwelling plume off northwest Africa in ocean color and sea surface temperature satellite imagery (Fig. 17). The upwelling plume off northwest Africa tends to have a southwestward direction. The bulk of the large *Sargassum* windrow that forms across the Atlantic is removed from the northwest Africa upwelling zone, except for the easternmost patches that overlap the Guinea Dome region (Fig. 17). The Guinea Dome is another important nutrient source for the *Sargassum* patches that aggregate under the ITCZ in the eastern tropical Atlantic.

5.3. Increases and variability in Sargassum concentrations in the tropical Atlantic since 2011

Lapointe (1986, 1995) quantified the growth of *Sargassum* in the presence of nutrients. Is there a source of nutrients for the *Sargassum* in the middle of the tropical Atlantic Ocean? In general, in the offshore tropical Atlantic, surface nutrient concentrations (nitrate, phosphate, or organic nutrients) are low to undetectable. However, concentrations of 2–4 μM nitrate are found within 40–50 m of the surface (NOAA World Ocean Atlas 2018). To determine whether *Sargassum* could benefit from these nutrients, we examined the seasonal and interannual variation in the MLD over the large area of formation of the *Sargassum* bloom. Fig. 1d shows the area-averaged time series of *Sargassum* coverage overlain on the daily time series (and monthly climatology) of the MLD

over the large area of formation of the *Sargassum* (2–5°N, 20–40°W).

The MLD has two deepening periods. The deepest MLD occurs around August (68 ± 5.4 m) every year; a secondary maximum occurs around October-December (55 ± 7.3 m). Thus, the MLD exceeds the typical depth of the nutricline in the tropical Atlantic, effectively entraining nutrients into the mixed layer. These nutrients would then be available to primary producers floating at the surface. This is a situation analogous to that of the classical spring bloom scenario (Gran and Braarud, 1935; Sverdrup, 1953; Menzel and Ryther, 1960; Dugdale and Goering, 1967; McKinley et al., 2000; Lipschultz et al., 2002).

Sargassum populations bloom in the tropical Atlantic in an area of active upward eddy-driven nutrient supply (McGillicuddy et al., 2003), during or shortly after the minima in MLD were observed (Fig. 1d). Interannual variations in the timing, structure, and depth of the MLD are important in the subsequent formation of the large *Sargassum* windrow under the ITCZ. Fig. 18a shows a strong correlation between the *Sargassum* density and the MLD. Our analysis demonstrates that the MLD in the tropical Atlantic is controlled by surface wind stress.

The tropical Atlantic has experienced a generally deep MLD at the end of the year and a progressively shallower MLD in the first few months of the year since 2011 (Fig. 1d). There has also been a tendency toward increasingly deeper MLD under the ITCZ and the *Sargassum* belt from 2010 to 2018 (Fig. 18a). The most intense *Sargassum* blooms were observed when the deepest MLD (and strongest trade winds) were also observed. When we examined the MLD time series in more detail, we noticed that when the MLD remained shallow relative to the climatology during October to December in the region 2–5°N, 20–40°W (Fig. 1d), such as occurred in 2012 and 2015, the bloom the following year is absent (as in 2013), or smaller and delayed (as in 2016). This is the region where the *Sargassum* bloom starts, as remnant populations of *Sargassum* aggregate when there is a strong wind convergence in April-May. This can also be seen for the MLD under the *Sargassum* belt (Fig. 18a). Indeed, the MLD was shallower than normal for several months in 2012–2013, before a minimum in *Sargassum* was observed in 2013.

Changes in the MLD likely affect the amount of nutrients available to *Sargassum* floating near the surface ocean. The climatological MLD was generally close to or deeper than the climatological nutricline, determined as the depth where nitrate > 0.5 μM (Fig. 18b). For most of the year, nitrate concentrations averaged within the MLD are higher than the nitrate in the upper 10 m (Fig. 18c). The deepening of the MLD in and around the ITCZ is an effective nutrient-delivery mechanism for *Sargassum* in the tropical Atlantic year-round, providing on the order of 33 mol km^{-2} per month to the bloom over the extent of the *Sargassum* belt. Note this is 1–3 orders of magnitude larger than the monthly supply of nitrate delivered by the Amazon plume if instantaneously dispersed over the area of the Amazon plume. The nutrients supplied by vertical mixing are, however, available over the full extent of the *Sargassum* belt. The *Sargassum* belt is not spatially coincident with the Amazon River plume for most of the year in the tropical Atlantic (Fig. 17). We suggest that vertical mixing and open-ocean upwelling are the most likely nutrient source supporting the increases in the standing stock of *Sargassum* in the tropical Atlantic that, in turn, have led to the massive inundations that affect communities in Africa, Brazil, and the Caribbean Sea. When winds are weak, such as during the last quarter of 2012, this results in a shallower MLD and less nutrient availability, and as a result the likelihood of a bloom the following spring diminishes, as was the case in 2013 when there was no significant bloom.

In addition to mixed layer dynamics entraining nutrients into the upper layers of the water column, there are also regions of upward vertical motions in the tropical Atlantic caused by the curl of the wind and associated Ekman pumping (Schott et al., 2004). For example, see the outline of upwelling velocities > 0.1 m d^{-1} in the sequence of Fig. 17 during June-October. While these are relatively weak upwelling velocities, they are in the right direction (upward) and thus contribute to the mixing of nutrients to the ocean surface when the MLD is shallow. Upwelling in the Guinea Dome region provides nutrients to large *Sargassum* patches in that area. But the rest of the region under the ITCZ, where the large *Sargassum* windrow forms across the Atlantic, is removed from that nutrient source (Fig. 17).

6. Summary and conclusions

Beginning in 2011 there have been unprecedented accumulations of *Sargassum* on the beaches of the Caribbean Sea, West Africa, and northeast Brazil. The biological and socioeconomic impacts of these *Sargassum* inundations have received a great deal of attention by the public as well as from scientific studies (e.g., Franks et al., 2016; Wang et al., 2019a; among many others). Our results offer an explanation for these events.

Fig. 19 is a schematic that attempts to summarize the processes of dispersal and recurrence of pelagic *Sargassum* accumulations in the tropical Atlantic. The schematic was drawn from a compilation of the results of the NCEP reanalysis, surface drifter analyses, and other data described above, as well as the results from previous studies. A sketch of the *Sargassum* accumulation observed in the MERIS satellite-based MCI
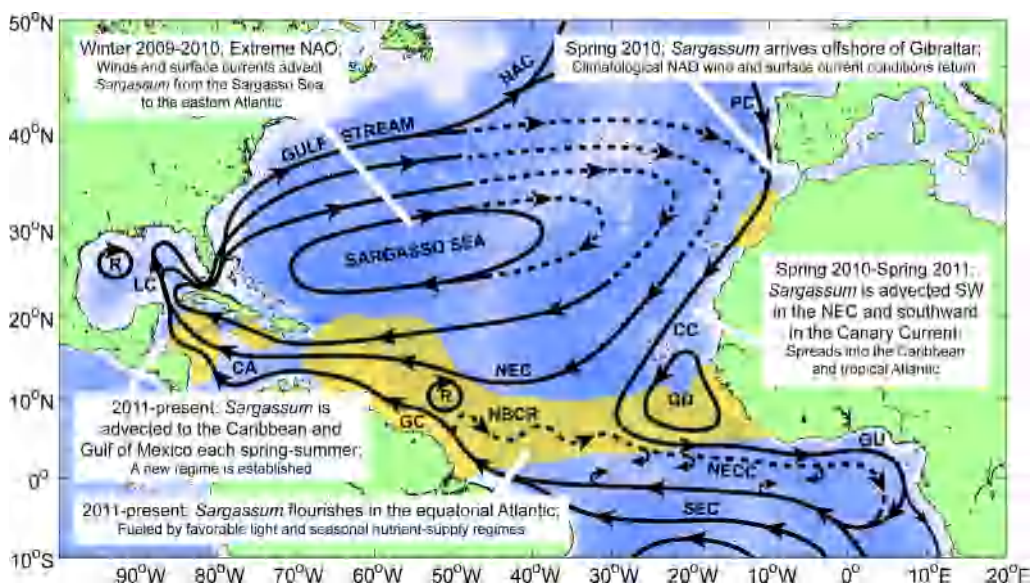
Fig. 19. Schematic portraying the hypothesized route that the *Sargassum* took to reach the tropics and the Caribbean Sea from the northeast Atlantic after the NAO wind anomaly ceased. This map shows conceptualized flow pathways drawn from the NCEP and drifter maps (the solid black lines indicate the climatological surface flow, while the dashed black lines indicate areas where there is variability from the climatology, such as the eastward flow between 30 and 40°N caused by the negative NAO, and the seasonally-reversing flow of the NBC retroflection and the NECC). The July 2011 *Sargassum* distribution in the tropical Atlantic during spring/summer 2011 from Gower et al. (2013) is superimposed on the flow pathways as the gold shaded areas. Please refer to the text in the paper for the definition of the acronyms.

images from spring/summer 2011 (gold patches; Gower et al., 2013) was overlain on the circulation streamlines. The circulation pathways shown include windage (direct wind forcing of water and *Sargassum* at the ocean's surface), which became more significant during the negative NAO event of 2009–2010. At that time, anomalous eastward winds advected the *Sargassum* farther east than usual, toward Gibraltar between the Iberian Peninsula and the Moroccan coast. The *Sargassum* served as a tracer of the changes caused by anomalous winds and associated windage.

In effect, a new equilibrium state may have now been reached for the *Sargassum* population of the Atlantic Ocean. The *Sargassum* population of the North Atlantic crossed a "tipping point" forced by the strong negative NAO event in winter 2009–2010. The elements of this tipping point and the consequences are as follows (Fig. 19):

a) Dispersal from the Sargasso Sea to the eastern Atlantic during the 2009–2010 winter NAO:
   o Changes in the winds over the North Atlantic strengthened and shifted the westerlies southward associated with an extreme negative NAO during December 2009 to March 2010;
   o Strong, persistent winds blew east across the Sargasso Sea towards Gibraltar and the Mediterranean Sea, causing the surface currents to flow to the east across the entire subtropical North Atlantic. Previous studies (e.g., Franks et al., 2016) either did not account for the effect of windage, or assumed a short duration of rafting (< 6 months) (e.g., Wang et al., 2019a);
   o The anomalous eastward winds and currents defined a new but temporary pathway for *Sargassum* to move eastward out of the Sargasso Sea and join the climatological southward-flowing Canary Current along the coast of West Africa.
b) Dispersal from the eastern Atlantic and entrainment into the central tropical Atlantic:
   o Once the NAO wind anomaly ceased at the end of March 2010, portions of the *Sargassum* population drifted southwestward in the NEC toward the Caribbean Sea while other portions joined the counter-clockwise flow around the Guinea Dome;
   o *Sargassum* was also entrained in the seasonal NECC in May-June 2010, spreading east into the Gulf of Guinea;
   o The key to understanding the redistribution of *Sargassum* is the incorporation of windage in the analysis of advection, which is also captured by undrogued drifters.
c) Establishment of a new, persistent tropical *Sargassum* population supported by wind convergence aggregation, surface currents, and mixed layer dynamics:
   o *Sargassum* now has a resident population in the central tropical Atlantic that aggregates in *trans*-Atlantic windrows under the action of the wind convergence that forms the ITCZ;
   o *Sargassum* starts to aggregate by convergent winds along the ITCZ during March-April; as the ITCZ migrates northward from May to September, the associated *Sargassum* windrow moves north with it;
   o The *Sargassum* accumulation under the ITCZ stretches eastward as the ITCZ crosses the latitude of formation of the North Equatorial Counter Current (NECC) in May-August every year. At this time, the western portion of the *Sargassum* belt also benefits from nutrients in the Amazon plume;
   o *Sargassum* continues to move north with the ITCZ in August and September, past the latitude of the NECC;
   o In October, when the ITCZ starts to move back south, the wind convergence weakens and loses its ability to concentrate the *Sargassum*. A large *Sargassum* row is left behind and remnant patches of the *Sargassum* population remain dispersed in the central tropical Atlantic around 10-15˚N;
   o The remnant dispersed patches of *Sargassum* provide a seed population for the accumulation under the ITCZ the following year;
   o In March-April, this new *Sargassum* aggregation shows enhanced growth supported by nutrients entrained in the upper water column.

The *Sargassum* patches and windrows are exposed to open-ocean upward diffusive flux of nutrients due to eddy and mixed layer dynamics. The mixed layer in the tropical Atlantic between about 2 and 5˚N deepens between August and December and then becomes shallower. Nutrients are available to *Sargassum* in a typical northern spring bloom scenario as the MLD becomes shallower and the water column becomes more stable in an area where there is active upward eddy diffusion of nutrients;
   o When winds in the tropical Atlantic are weaker than normal, the mixed layer does not reach its climatological maximum, and *Sargassum* does not bloom as intensively in the following 3–6 months. In particular, if the wind convergence is weaker than normal, *Sargassum* remnant patches do not bloom and do not survive February-March. They also do not aggregate under the ITCZ, and/or the bloom is weaker or delayed;
   o Open-ocean upwelling due to the wind stress curl may be a small additional source of nutrients, as it may bring the nutricline closer to the surface and into the surface mixed layer;
   o Eddy diffusion and surface layer mixing are important nutrient sources that are complemented by the Amazon and Orinoco Rivers and African upwelling.

Our results explain the unprecedented spread and accumulation of vegetative biomass in the tropical Atlantic through the long-distance dispersal of *Sargassum* from the North Atlantic. Key traits of organisms are as important as ocean physics when modeling movements of marine organisms. Both shape the inferences made regarding the drivers of biogeographic patterns (Brooks et al., 2018; Putman et al., 2018). Our work shows that models of transport need not be particularly complex, but must capture key elements of the system, especially long drift times and exposure to the winds at the surface in the case of *Sargassum* movement, to be able to understand biological processes in the marine environment.

However, many questions remain. Was the extreme and prolonged negative NAO during winter 2009–2010 part of natural climate variability, or can there be attribution to anthropogenic effects? Did similar *Sargassum* "invasions" occur in the past, and how long will this one last? How might the present *Sargassum* rafts and mats affect fish and other species that associate with them? Can mitigating actions be taken, and if the *Sargassum* can be harvested, are there potentially uses or applications for *Sargassum*-derived products?

The question of whether conditions that led to the *Sargassum* redistribution were due to short-term natural variability or to changes in climate is important in the context of the high value of coastal and marine resources (e.g., Fisheries Economics of the United States, NMFS, 2018). Extreme variability in environmental conditions has long been attributed to climate change (e.g., Muller-Karger, 1993). More recently, methods to estimate attribution of extreme weather events to human-induced climate have included regime-based (e.g., Cattiaux et al., 2010) and odds-based – Fraction of Attributable Risk – approaches (e.g., Stott et al., 2016). Attribution studies in the marine environment are relatively new (e.g., Jacox et al., 2017; Webb and Werner, 2017). Despite these analytical advances, climate attribution remains in some cases nuanced (e.g., Herring et al., 2019, and references therein). Relevant to our study, Deser et al. (2016) note that the NAO is primarily controlled by intrinsic atmospheric dynamics, constituting a major source of unpredictable natural variability whose impacts will be superimposed upon those of anthropogenic climate change. Thus, future (and past) climate trends in regions affected by the NAO are best conveyed in terms of an expected range that incorporates both the natural variability and the forced climate change signal. For example, Cattiaux et al.'s (2010) analyses suggested that the extreme cold 2010 European winter – estimated to be within the expected natural variability – was mitigated by long-term warming. While the question of the role of climate in events such as those associated with the extreme low 2009–2010 NAO remains, we cannot at this point robustly estimate the

relative contributions of the natural/intrinsic variability of the NAO and its interactions with long-term forcing conditions.

We also cannot say that similar *Sargassum* "invasion" events have not occurred prior to these recent episodes. Webster and Linton (2013) chronicled episodic occurrences of *Sargassum* along the Texas Gulf coast since the late 1800's. As such, we should expect that episodes occurred in other parts of the Gulf of Mexico and the Caribbean but we have not found other reports describing such events.

How long will the present tropical Atlantic/Caribbean episode last? Will it become a permanent regime or new baseline? The answer depends on whether sufficient *Sargassum* standing stock remains after each season to re-aggregate and bloom again. This depends on possible flushing and residence times, wind mixing, and nutrient supply mechanisms in the region. It is possible that one or more years such as the 2013 nutrient limitation event, which was related to shallow MLD conditions, can return the *Sargassum* distribution to pre-2010 conditions and end the present nuisance *Sargassum* blooms. Sustained monitoring is required to understand the phenomenon better and assess any possible trends.

The socio-ecological impact of the increased presence of *Sargassum* is multi-faceted. The ecological importance of *Sargassum* rafts and mats for hundreds of species – invertebrates and fish – has long been known (e.g., Wells and Rooker, 2004; UNEP, 2015; UNEP, 2018; and references therein). As such, the increased presence of *Sargassum* – in its pelagic phase – could have beneficial effects for protected species (e.g., turtles; Witherington et al., 2012), recruitment of commercial fished species (e.g., gray triggerfish; Burton et al., 2015), etc. In contrast, beached or near-shore accumulations of *Sargassum* can have detrimental effects. Coastal accumulations of *Sargassum* can affect nesting areas for turtles (e.g., Maurer et al., 2015), and the arrival and accumulations of large amounts of *Sargassum* were found to cause mortalities through the combined effects of high ammonium and hydrogen sulfide concentrations, together with hypoxic conditions along the Mexican Caribbean coast (e.g., Rodríguez-Martínez et al., 2019). Continued arrival and decay of pelagic *Sargassum* can also affect local water quality and affect near-shore coral reefs and seagrass beds (van Tussenbroek et al., 2017). These effects suggest consideration of engineering solutions, such as construction of barriers, or possibly harvesting *Sargassum* for biochemicals, feed, food, fertilizer, and fuel (e.g., Marín et al., 2009; Milledge and Harvey, 2016).

Continued further interdisciplinary study of the unique, dynamic, and changeable pelagic *Sargassum* ecosystem will be needed for it to be fully understood and to improve predictions of its distribution and impacts.

Declaration of Competing Interest

Acknowledgments

References

Allshouse, M.R., Ivey, G.N., Lowe, R.J., Jones, N.L., Beegle-Krause, C.J., Xu, J., Peacock, T., 2016. Impact of windage on ocean surface Lagrangian coherent structures. Environ. Fluid Mech. NA 1–11. https://doi.org/10.1007/s10652-016-9499-3.

Baez, J.C., Salvo, A.E., Flores-Moya, A., 2016. Persistent golden tides stranding Caribbean Sea in 2014 and 2015. Harmful Algal News, No. 52, 4.

Bakun, A., 1973. Coastal Upwelling Indices, West Coast of North America, 1946–1971; NOAA Technical Report NMFS SSRF-671; U.S. Department of Commerce: Washington, DC, USA, 1973; p. 103.

Blomquist, H.L., Pyron, J.H., 1943. Drifting "Seaweed" at Beaufort, North Carolina. Am. J. Bot. 30 (1), 28–32.

Bonjean, F., Lagerloef, G.S.E., 2002. Diagnostic model and analysis of the surface currents in the tropical Pacific Ocean. J. Phys. Oceanogr. 32, 2938–2954.

Brooks, M.T., Coles, V.J., Hood, R.R., Gower, J.F.R., 2018. Factors controlling the seasonal distribution of pelagic *Sargassum*. Mar. Ecol. Prog. Ser. 599, 1–18.

Brooks, M.T., Coles, V.J., Coles, W.C., 2019. Inertia influences pelagic *Sargassum* advection and distribution. Geophys. Res. Lett. 46 (5), 2610–2618.

Brown, J., 1991. The final voyage of Rapaiti – A measure of sea-surface drift velocity in relation to the surface wind. Mar. Pollut. Bull. 22 (1), 37–40.

Bruce, J.G., 1984. Comparison of eddies off the North Brazilian and Somali Coasts. J. Phys. Oceanogr. 14 (4), 825–832.

Burton, M.L., Potts, J.C., Carr, D.R., Cooper, M., Lewis, J., 2015. Age, growth, and mortality of gray triggerfish (*Balistes capriscus*) from the southeastern United States. Fisheries Bull. 113 (1), 27–39. https://doi.org/10.7755/FB.113.1.3.

Carton, J.A., Zhou, Z.X., 1997. Annual cycle of sea surface temperature in the tropical Atlantic Ocean. J. Geophys. Res. 102, 27813–27824.

Cattiaux, J., Vautard, R., Cassou, C., Yiou, P., Masson-Delmotte, V., Codron, F., 2010. Winter 2010 in Europe: A cold extreme in a warming climate. Geophys. Res. Lett. 37, L20704. https://doi.org/10.1029/2010GL044613.

Chassignet, E.P., Hurlburt, H.E., Smedstad, O.M., Halliwell, G.R., Hogan, P.J., Wallcraft, A.J., Baraille, R., Bleck, R., 2007. The HYCOM (Hybrid Coordinate Ocean Model) data assimilative system. J. Mar. Syst. 65, 60–83.

Chereskin, T.K., Price, J.F., 2001. Ekman Transport and Pumping. Elsevier Ltd. 1st edition of Encyclopedia of Ocean Sciences, vol. 2, pp. 809–815.

Collins, F.S., 1917. The Sargasso Sea. J. N. Engl. Botanical Club 19 (221), 77–84.

Colna, K.E., 2017. Latitudinal Position and Trends of the Intertropical Convergence Zone (ITCZ) and its Relationship with Upwelling in the Southern Caribbean Sea and Global Climate Indices. Graduate Theses and Dissertations, http://scholarcommons.usf.edu/etd/6645.

Connor, J.L., Adey, W.H., 1977. The Benthic Algal Composition, Standing Crop, and Productivity of a Caribbean Algal Ridge. Atoll Research Bulletin, pp. 211.

Coston-Clements, L., Settle, L.R., Hoss, D.E., Cross, F.A., 1991. Utilization of the Sargassum habitat by marine invertebrates and vertebrates – A review. NOAA Technical Memorandum NMFS-SEFSC-296, 32 pp.

Dakos, V., Matthews, B., Hendry, A.P., Levine, J., Loeuille, N., Norberg, J., Nosil, P., Scheffer, M., De Meester, L., 2019. Ecosystem tipping points in an evolving world. Nat. Ecol. Evol. 3, 355–362.

Deser, C., Hurrell, J.W., Phillips, A.S., 2016. The role of the North Atlantic Oscillation in European climate projections. Clim. Dyn. https://doi.org/10.1007/s00382-016-3502-z.

Dixon, C.C., 1925. The Sargasso Sea. The Geographical J. 66 (5), 434–442.

Djakouré, S., Araujo, M., Hounsou-Gbo, A., Noriega, C., Bourlès, B., 2017. On the potential causes of the recent Pelagic *Sargassum* blooms events in the tropical North Atlantic Ocean. Biogeosci. Discuss. https://doi.org/10.5194/bg-2017-346.

Duffy, J.E., Benedetti-Cecchi, L., Trinanes, J.A., Muller-Karger, F.E., Ambo-Rappe, R., Boström, C., Buschmann, A.H., Byrnes, J., Coles, R.G., Creed, J., Cullen-Unsworth, L., 2019. Toward a coordinated global observing system for seagrasses and marine macroalgae. Front. Mar. Sci. 6, 317.

Dugdale, R.C., Goering, J.J., 1967. Uptake of new and regenerated forms of nitrogen in primary productivity. Limnol. Oceanogr. 12, 196–206.

ESR, 2009. OSCAR third degree resolution ocean surface currents. Ver. 1. PO.DAAC, CA,

USA. 10.5067/OSCAR-03D01.

Foltz, G.R., Brandt, P., Richter, I., Rodriguez-Fonseca, B., Hernandez, F., Dengler, M., Rodriguez, R.R., Schmidt, J.O., Yu, L., Lefevre, N., Cotrim Da Cunha, L., McPhaden, M.J., Araujo, M., Karstensen, J., Hahn, J., Martin-Rey, M., Patricola, C.M., Poli, P., Zuidema, P., Hummels, R., Perez, R.C., Hatje, V., Lubbecke, J.F., Polo, I., Lumpkin, R., Bourles, B., Asuquo, F.E., Lehodey, P., Conchon, A., Chang, P., Dandin, P., Schmid, C., Sutten, A., Giordani, H., Xue, Y., Illig, S., Losada, T., Grodsky, S.A., Gasparin, F., Lee, T., Mohino, E., Nobre, P., Wanninkhof, R., Keenlyside, N., Garcon, V., Sanchea-Gomez, E., Nnamchi, H.C., Drevillon, M., Storto, A., Remy, E., Lazar, A., Speich, S., Goes, M., Dorrington, T., Johns, W.E., Moum, J.N., Robinson, C., Perruche, C., de Souza, R.B., Gaye, A.T., Lopez-Parages, J., Moneries, P.-A., Castellanos, P., Benson, N.U., Houkonnou, M.N., Trotte Duha, J., Laxenaire, R., Reul, N., 2019. The tropical atlantic observing system. Front. Mar. Sci. https://doi.org/10.3389/fmars.2019.00206.

Franks, J.S., Johnson, D.R., Ko, D.S., Sanchez-Rubio, G., Hendon, J.R., Lay, M., 2011. Unprecedented influx of pelagic Sargassum along Caribbean island coastlines during summer 2011. In: Proceedings of the 64th Gulf and Caribbean Fishery Institute, Puerto Morelos, Mexico, November 2011, extended abstract, 4 pp.

Franks, J.S., Johnson, D.R., Ko, D.S., 2016. Pelagic *Sargassum* in the tropical North Atlantic. Gulf Caribbean Res. 27, SC6-11.

Fraser, C.I., Morrison, A.K., Hogg, A.M., Macaya, E.C., van Sebille, E., Ryan, P.G., Padovan, A., Jack, C., Valdivia, N., Waters, J.M., 2018. Antarctica's ecological isolation will be broken by storm-driven dispersal and warming. Nat. Clim. Change 8, 704–708.

Gavio, B., Rincón-Diaz, M.N., Santos-Martínez, A., 2015. Massive quantities of pelagic *Sargassum* on the shores of San Andres island, southwestern Caribbean. Acta Biol. Colomb. 20 (1), 239–241.

Glynn, P.E., Almodóvar, L.R., González, J.G., 1964. Effects of Hurricane Edith on marine life in La Parguera, Puerto Rico. Caribbean J. Sci. 4 (2&3), 335–345.

Gower, J., Hu, C., Borstad, G., King, S., 2006. Ocean color satellites show extensive lines of floating *Sargassum* in the Gulf of Mexico. IEEE Trans. Geosci. Remote Sens. 44 (12), 3619–3625.

Gower, J., King, S., 2008. Satellite images show the movement of floating *Sargassum* in the Gulf of Mexico and Atlantic Ocean. Nat. Precedings hdl:10101/npre.2008.1894.1, 13.

Gower, J.F.R., King, S.A., 2011. Distribution of floating *Sargassum* in the Gulf of Mexico and the Atlantic Ocean mapped using MERIS. Int. J. Remote Sens. 32 (7), 1917–1929.

Gower, J., Young, E., King, S., 2013. Satellite images suggest a new *Sargassum* source region in 2011. Remote Sens. Lett. 4 (8), 764–773.

Gran, H.H., Braarud, T., 1935. A Quantitative Study of the Phytoplankton in the Bay of Fundy and the Gulf of Maine (including observations on hydrography, chemistry and turbidity. J. Biol. Board Canada 1 (5), 279–467. https://doi.org/10.1139/f35-012.

Grodsky, S.A., Carton, J.A., McClain, C.R., 2008. Variability of upwelling and chlorophyll in the equatorial Atlantic. Geophys. Res. Lett. 35 (3). https://doi.org/10.1029/2007GL032466.

Hanisak, M.D., Samuel, M.A., 1987. Growth rates in culture of several species of *Sargassum* from Florida, USA. In: Ragan, M.A., Bird, C.J. (Eds.), Twelfth International Seaweed Symposium. Developments in Hydrobiology. Springer, Dordrecht.

Herring, S.C., Christidis, N., Hoell, A., Hoerling, M., Stott, P.A., 2019. Introduction to explaining extreme events of 2017 from a climate perspective. Bull. Am. Meteorol. Soc. 100 (1), S1–S3. https://doi.org/10.1175/BAMS-D-18-0307.1.

Hu, C., Montgomery, E.T., Schmitt, R.W., Muller-Karger, F.E., 2004. The Amazon and Orinoco River plumes in the tropical Atlantic and Caribbean Sea: Observation from space and S-PALACE floats. Deep-Sea Res. Part II. Topical Studies Oceanography 51(10–11), 1151–1171.

Hughes, P., 1956. A determination of the relation between wind and sea-surface drift. Q. J. R. Meteorolog. Soc. 82 (354), 494–502.

Hurrell, J.W., Deser, C., 2009. North Atlantic climate variability: The role of the North Atlantic Oscillation. J. Mar. Syst. 78, 28–41.

Inui, T., Lazar, A., Malanotte-Rizzoli, P., Busalacchi, A., 2002. Wind stress effects on subsurface pathways from the subtropical to tropical Atlantic. J. Phys. Oceanogr. https://doi.org/10.1175/1520-0485(2002) 032 < 2257:WSEOSP > 2.0.CO;2.

Jacox, M.G., Alexander, M.A., Mantua, N.J., Scott, J.D., Hervieux, G., Webb, R.S., Werner, F.E., 2017. Forcing of multiyear extreme ocean temperatures that impacted California current living marine resources in 2016 [in "explaining extreme events of 2016 from a climate perspective"]. Bull. Am. Meteorological Soc. 98 (12), S27–S33. https://doi.org/10.1175/BAMSD-17-0119.1.

Johns, E.M., Muhling, B.A., Perez, R.C., Muller-Karger, F.E., Melo, N., Smith, R.H., Lamkin, J.T., Gerard, T.L., Malca, E., 2014. Amazon River water in the northeastern Caribbean Sea and its effect on larval reef fish assemblages during April 2009. Fish. Oceanogr. 23 (6), 472–494.

Johnson, D.R., Ko, D.S., Franks, J.S., Moreno, P., Sanchez-Rubio, G., 2012. The Sargassum invasion of the eastern Caribbean and dynamics of the equatorial North Atlantic. In: Proceedings of the 65th Gulf and Caribbean Fisheries Institute, November 5-9, 2012, Santa Marta, Colombia, extended abstract.

Johnson, D.L., Richardson, P.L., 1977. On the wind-induced sinking of *Sargassum*. J. Exp. Mar. Biol. Ecol. 28, 255–267.

Kalnay, E., Kanamitsu, M., Kistler, R., Collins, W., Deaven, D., Gandin, L., Iredell, M., Saha, S., White, G., Woollen, J., Zhu, Y., Chelliah, M., Ebisuzaki, W., Higgins, W., Janowiak, J., Mo, K.C., Ropelewski, C., Wang, J., Leetmaa, A., Reynolds, R., Jenne, R., Joseph, D., 1996. The NCEP/NCAR 40-year reanalysis project. Bull. Am. Meteorol. Soc. 77 (3), 437–471.

Kara, A.B., Rochford, P.A., Hurlburt, H.E., 2000. An optimal definition for ocean mixed layer depth. J. Geophys. Res. 105 (C7), 16803–16821. https://doi.org/10.1029/2000JC900072.

Kara, A.B., Rochford, P.A., Hurlburt, H.E., 2003. Mixed layer depth variability over the

global ocean. J. Geophys. Res. 108 (C3), 3079. https://doi.org/10.1029/2000JC000736.

Katz, E.J., 1981. Dynamic topography of the sea surface in the equatorial Atlantic. J. Mar. Res. 39, 53–63.

Kessler, W.S., 2006. The circulation of the eastern tropical Pacific: A review. Prog. Oceanogr. 69, 181–217.

Kistler, R., Kalnay, E., Collins, W., Saha, S., White, G., Woollen, J., Chelliah, M., Ebisuzaki, W., Kanamitsu, M., Kousky, V., van den Dooi, H., Jenne, R., Fiorino, M., 2001. The NCEP-NCAR 50-year reanalysis: Monthly means CD-ROM and documentation. Bull. Am. Meteorol. Soc. 82 (2), 247–267.

Komoe, K., Sankare, Y., Fofie, N'G.B.Y., Bamba, A., Sahr, A.G.-S., 2016. Taxonomic study of two species of *Sargassum*: *Sargassum fluitans* (Borgesen) Borgesen and *Sargassum natans* (Linnaeus) Gaillon (brown algae) collected in Cote d'Ivoire coasts, West Africa. Nat. Sci. 14 (10), 50–56.

Laffoley, D.d'A., Roe, H.S.J., Angel, M.V., Ardron, J., Bates, N.R., Boyd, I.L., Brooke, S., Buck, K.N., Carlson, C.A., Causey, B., Conte, M.H., Christiansen, S., Cleary, J., Donnelly, J., Earle, S.A., Edwards, R., Gjerde, K.M., Giovannoni, S.J., Gulick, S., Gollock, M., Hallet, J., Halpin, P., Hanel, R., Hemphill, A., Johnson, R.J., Knap, A.H., Lomas, M.W., McKenna, S.A., Miller, M.J., Miller, P.I., Ming, F.W., Moffitt, R., Nelson, N.B., Parson, L., Peters, A.J., Pitt, J., Rouja, P., Roberts, J., Seigel, D.A., Siuda, A.N.S., Steinberg, D.K., Stevenson, A., Sumaila, V.R., Swartz, W., Thorrold, S., Trott, T.M., Vats, V., 2011. The protection and management of the Sargasso Sea: The golden floating rainforest of the Atlantic Ocean. Summary Science and Supporting Evidence Case, Sargasso Sea Alliance 44.

Lamb, J., 2018. The Great Seaweed Invasion. JSTOR weekly digest, October 24, 2018. Accessed on 11/20/2018 at https://daily.jstor.org/great-seaweed-invasion/.

Lapointe, B.E., 1986. Phosphorus-limited photosynthesis and growth of *Sargassum natans* and *Sargassum fluitans* (Phaeophyceae) in the western North Atlantic. Deep-Sea Res. 33 (3), 391–399.

Lapointe, B.E., 1995. A comparison of nutrient-limited productivity in *Sargassum natans* from neritic vs. oceanic waters of the western North Atlantic Ocean. Limnol. Oceanogr. 40 (3), 625–633.

Lett, C., Verley, P., Mullon, C., Parada, C., Brochier, T., Penven, P., Blanke, B., 2008. A Lagrangian tool for modelling ichthyoplankton dynamics. Environ. Modell. Software 23, 1210–1214.

Lipschultz, F., Bates, N., Carlson, C., Hansell, D., 2002. New production in the Sargasso Sea: History and current status. Global Biogeochem. Cycles 16. https://doi.org/10.1029/2000GB001319.

Lumpkin, R., Garzoli, S., 2005. Near-surface circulation in the tropical Atlantic Ocean. Deep-sea Res. I 52, 495–518.

Lumpkin, R., Pazos, M., 2007. Measuring surface currents with Surface Velocity Program drifters: the instrument, its data, and some recent results. In: Mariano, A., Rossby, T., Kirwan, D. (Eds.), Chapter 2 of: Lagrangian Analysis and Prediction of Coastal and Ocean Dynamics. Cambridge University Press, pp. 23.

Lumpkin, R., Grodsky, S.A., Centurioni, L., Rio, M.-H., Carton, J.A., Lee, D., 2013. Removing spurious low-frequency variability in drifter velocities. J. Atmos. Oceanic Technol. 30, 353–360.

Lumpkin, R., Centurioni, L., Perez, R.C., 2016. Fulfilling observing system implementation requirements with the global drifter array. J. Atmos. Oceanic Technol. 33, 685–695.

Marín, A., Casas-Valdez, M., Carrillo, S., Hernández, H., Monroy, A., Sanginés, L., Pérez-Gil, F., 2009. The marine algae *Sargassum* spp. (Sargassaceae) as feed for sheep in tropical and subtropical regions. Revista de Biologia Tropical 57, 1271–1281.

Martin, L.M., 2016. Pelagic Sargassum and its associated mobile fauna in the Caribbean, Gulf of Mexico, and Sargasso Sea. Master of Science Thesis, Texas A&M University, 87 pp.

Maurer, A.S., De Neef, E., Stapleton, S.P., 2015. *Sargassum* accumulation may spell trouble for nesting sea turtles. Front. Ecol. Environ. 13, 394–395.

McGillicuddy Jr., D.J., Anderson, L.A., Doney, S.C., Maltrud, M.E., 2003. Eddy-driven sources and sinks of nutrients in the upper ocean: results from a 0.1∘ resolution model of the North Atlantic. Global Biogeochem. Cycles 17, 1035. https://doi.org/10.1029/2002GB001987.

McKinley, G.A., Follows, M.J., Marshall, J., 2000. Interannual variability of the air-sea flux of oxygen in the North Atlantic. Geophys. Res. Lett. 27, 1933–2936.

Menemenlis, D., Campin, J., Heimbach, P., Hill, C., Lee, T., Nguyen, A., Schodlock, M., Zhang, H., 2008. ECCO2: high resolution global ocean and sea ice data synthesis. Mercator Ocean Quarterly Newsletter 31, 13–21.

Menzel, D.W., Ryther, J.H., 1960. The annual cycle of primary production in the Sargasso Sea off Bermuda. Deep-Sea Res. 6, 351–367.

Milledge, J.J., Harvey, P.J., 2016. Golden tides: problem or golden opportunity? The valorization of *Sargassum* from beach inundations. J. Mar. Sci. Eng. 4 (3), 60. https://doi.org/10.3390/jmse4030060.

Mittelstaedt, E., 1991. The ocean boundary along the north Africa coast: Circulation and oceanographic properties at the sea surface. Prog. Oceanogr. 26, 307–355.

Montégut, C.de B., Madec, G., Fischer, A.S., Lazar, A., Ludicone, D., 2004. Mixed layer depth over the global ocean: An examination of profile data and a profile-based climatology. J. Geophys. Res.: Oceans 109 https://doi.org/10.1029/2004JC002378. C12003.

Moreira, A., Alfonso, G., 2013. Inusual arribazón de *Sargassum fluitans* (Borgesen) Borgesen en la costa centro-sur de Cuba. Revista de Investigaciones Marinas 33 (2), 17–20.

Muller-Karger, F.E., McClain, C.R., Richardson, P.L., 1988. The dispersal of the Amazon's water. Nature 333, 56–59.

Muller-Karger, F.E., 1993. River discharge variability including satellite-observed plume-dispersal patterns. United Nations Environmental Programme (Wider Caribbean Region) and Intergovernmental Oceanographic Commissions (Caribbean and

Adjacent Regions) In: Maul, George (Ed.), Climate Change in the Intra-Americas Sea. Edward Arnold Publishers, pp. 162–192.

Muller-Karger, F.E., Richardson, P.L., McGillicuddy, D., 1995. On the offshore dispersal of the Amazon's Plume in the North Atlantic. Deep-Sea Res. I 42 (11/12), 2127–2137.

Muller-Karger, F.E., Smith, J.P., Werner, S., Chen, R., Roffer, M., Liu, Y., Muhling, B., Lindo-Atichati, D., Lamkin, J., Cerdeira-Estrada, S., Enfield, D.B., 2015. Natural variability of surface oceanographic conditions in the offshore Gulf of Mexico. Prog. Oceanogr. https://doi.org/10.1016/j.pocean.2014.12.007.

NASA/GSFC/NOAA, 2009. Cross-Calibrated Multi-Platform Ocean Surface Wind Vector L3.0 First-Look Analyses, Ver. 1, PO.DAAC, CA, USA, Dataset accessed at 10.5067/CCF30-01XXX.

NMFS, 2018. Fisheries Economics of the United States 2016. U.S. Dept. of Commerce, NOAA Tech. Memo, NMFS-F/SPO-187, 243 pp, https://www.fisheries.noaa.gov/webdam/download/97729452.

NOAA, 2016. Report on Modeling Oceanic Transport of Floating Marine Debris. Silver Spring, MD, 21 pp.

Oey, L.Y., Ezer, T., Wang, D.P., Fan, S.J., Yin, X.Q., 2006. Loop current warming by Hurricane Wilma. Geophys. Res. Lett. 33, 8.

Oey, L.Y., Ezer, T., Wang, D.P., Fan, S.J., Yin, X.Q., 2007. Hurricane-induced motions and interaction with ocean currents. Cont. Shelf Res. 27, 1249–1263.

Oviatt, C.A., Huizenga, K., Rogers, C.S., Miller, W.J., 2019. What nutrient sources support anomalous growth and the recent *Sargassum* mass stranding on Caribbean beaches? A review. Mar. Pollut. Bull. 145, 517–525.

Parr, A.E., 1939. Quantitative observations on the pelagic *Sargassum* vegetation of the western North Atlantic – with preliminary discussion of morphology and relationships. Bull. Bingham Oceanographic Collection 6 (article 7), 94.

Putman, N.F., Lumpkin, R., Sacco, A.E., Mansfield, K.L., 2016. Passive drift or active swimming in marine organisms? Proc. R. Soc. B 283, 9.

Putman, N.F., Goni, G.J., Gramer, L.J., Hu, C., Johns, E.M., Trinanes, J., Wang, M., 2018. Simulating transport pathways of *Sargassum* from the Equatorial Atlantic into the Caribbean Sea. Prog. Oceanogr. 165, 205–214.

Reverdin, G., Delécluse, P., Lévy, C., Andrich, P., Morlière, A., Verstraete, J.M., 1991. The near surface tropical Atlantic in 1982–1984: Results from a numerical simulation and a data analysis. Prog. Oceanogr. 27, 273–340.

Richardson, P.L., Arsenault, S., Garzoli, S., Bruce, J., 1992. Annual cycle of the Atlantic North equatorial countercurrent. Deep-Sea Res. 39 (6), 997–1014.

Rodríguez-Martínez, R.E., Medina-Valmaseda, A.E., Blanchon, P., Monroy-Velázquez, L.V., Almazán-Becerril, A., Delgado-Pech, B., Vásquez-Yeomans, L., Francisco, V., García-Rivas, M.C., 2019. Faunal mortality associated with massive beaching and decomposition of pelagic *Sargassum*. Mar. Pollut. Bull. 146, 201–205.

Sánchez-Garrido, J.C., Werner, F., Ramos, A., Fiechter, J., Curchitser, E., Rose, K.A., García-Lafuente, J., Arístegui, J., Hernández-León, S., Rodríguez Santana, A., 2019. Decadal-scale variability of sardine and anchovy simulated with an end-to-end coupled model of the canary current ecosystem. Prog. Oceanography 171, 212–230. https://doi.org/10.1016/j.pocean.2018.12.009.

Sanchez-Rubio, G., Perry, H., Franks, J.S., Johnson, D.R., 2018. Occurrence of pelagic *Sargassum* in waters of the U.S. Gulf of Mexico in response to weather-related hydrographic regimes associated with decadal and interannual variability in global climate. Fish. Bull. 116 (1), 93–106.

Schell, J.M., Goodwin, D.S., Siuda, A.N.S., 2015. Recent *Sargassum* inundation events in the Caribbean – Shipboard observations reveal dominance of a previously rare form. Oceanography 28 (3), 8–10.

Schmitt, R., 2000. The Ocean's Role in Climate - Testimony to the Senate Committee on Commerce, Science, and Transportation. Woods Hole Oceanographic Institution (WHOI), July 18, 2000. https://www.whoi.edu/page.do?pid=8916&tid=7342&cid=24777.

Schott, F.A., McCreary Jr., J.P., Johnson, G.C., 2004. Shallow overturning circulations of the tropical-subtropical oceans. In: Wang, C., Xie, S.P., Carton, J.A. (Eds.), Earth Climate: The Ocean-Atmosphere Interaction. Geophysical Monograph Series 147. American Geophysical Union 10.1029/147GM15.

Sea Education Association (2006-2016). Compilation of net tow data from S. E. A. Final Cruise Reports: C207 (Chuck Lea 2006), C209 (Amy NS Siuda 2007), C210 (Giora Proskurowski 2007), C211 (Chuck Lea 2007), C213 (Chuck Lea 2007), C215 (Jeffrey M Schell 2008), C216 (Erik Zettler 2008), C219 (Jeffrey M Schell 2008), C222 (Jeffrey M Schell 2009), C223 (Chuck Lea 2009), C225 (Jeffrey M Schell 2009), C226 (Rick Murray 2009), C227 (Amy NS Siuda 2010), C228 (Jeffrey M Schell 2010), C229 (Amy NS Siuda 2010), C231 (Deborah Goodwin 2010), C232 (Amy NS Siuda 2010), C233 (Heather Schrum 2011), C234 (Jeffrey M Schell 2011), C237 (Chuck Lea 2011), C238 (Jeffrey M Schell 2011-12), C239 (Mary Engels 2012), C240 (Jeffrey M Schell 2012), C241 (Amy NS Siuda 2012), C243 (Chuck Lea 2012), C244 (Jeffrey M Schell 2013), C245 (Chuck Lea 2013), C246 (Jeffrey M Schell 2013), C247 (Amy NS Siuda 2013), C249 (Chuck Lea 2013), C250 (Jeffrey M Schell 2013), C251 (Chuck Lea 2013), C252 (Amy NS Siuda 2014), C256 (Jeffrey M Schell 2014), C257 (Jeffrey M Schell 2015), C259 (Amy NS Siuda 2015), C263 (Amy NS Siuda 2015), C264 (Jeffrey M Schell 2015), and C266 (Amy NS Siuda 2016). Sea Education Association, P. O. Box 6, Woods Hole, MA 02543, USA.

Sissini, M.N., de Barros Barreto, M.B.B., Szechy, M.T.M., de Lucena, M.B., Oliveira, M.C., Gower, J., Liu, G., de Oliveira Bastos, E., Milstein, D., Gusmao, F., Martinelli-Filho, J.E., Alves-Lima, C., Colepicolo, P., Ameka, G., de Graft-Johnson, K., Gouvea, L., Torrano-Silva, B., Nauer, F., J. Marcos de Castro Nunes, Barufi, J.B., 2017. The floating *Sargassum* (Phaeophyceae) of the South Atlantic Ocean – likely scenarios. Phycologia 56 (3), 321–328.

Smetacek, V., Zingone, A., 2013. Green and golden seaweed tides on the rise. Nature 504, 84–88.

Smith, R.L., 1968. Upwelling. Oceanography Mar. Biol. Ann. Rev. 6, 11–46.

Smith, T.M., York, P.H., Broitman, B.R., Thiel, M., Hays, G.C., van Sebille, E., Putman,

N.F., Macreadie, P.I., Sherman, C.D., 2018. Rare long-distance dispersal of a marine angiosperm across the Pacific Ocean. Glob. Ecol. Biogeogr. 27, 487–496.

Stewart, R.H., 2008. Introduction to Physical Oceanography. Department of Oceanography, Texas A &M University. Copyright 2008, September 2008 Edition, 358 pp., https://www.colorado.edu/oclab/sites/default/files/attached-files/stewart_textbook.pdf.

Stramma, L., Schott, F., 1999. The mean flow field of the tropical Atlantic Ocean. Deep-Sea Res. II 46, 27–303.

Stott, P.A., Christidis, N., Otto, F.E.L., Sun, Y., Vanderlinden, J.P., van Oldenborgh, G.J., Vautard, R., von Storch, H., Walton, P., Yiou, P., Zwiers, F.W., 2016. Attribution of extreme weather and climate-related events. WIREs Clim. Change 7, 23–41.

Sverdrup, H.U., 1953. On conditions for the vernal blooming of phytoplankton. Journal du Conseil International pour l'Exploration de la Mer 18, 287–295. https://doi.org/10.1093/icesjms/18.3.287.

Sverdrup, H.U., Johnson, M.W., Fleming, R.H., 1942. The Oceans - Their Physics, Chemistry, and General Biology. Prentice-Hall, Inc., Englewood Cliffs, N. J., USA.

Tomczak, G., 1964. Investigations with a large number of drift cards to determine the influence of the wind on surface currents. Stud. Oceanography 1964, 29–139.

UNEP, 2015. Concept note on the invasion of pelagic Sargassum in West Africa. UNEP Abidjan Convention, United Nations Environment Programme, September 2015. http://www.sargassoseacommission.org/storage/Concept_Note_on_Sargassum_Invasion_in_ West_Africa_-_UNEP_Abidjan_Convention_Secretariat.pdf.

UNEP, 2018. Sargassum White Paper - Sargassum Outbreak in the Caribbean: Challenges, Opportunities and Regional Situation. http://gefcrew.org/carrcu/SPAWSTAC8/Info-Docs/WG.40_INF8-en.pdf.

van Nes, E.H., Arani, B.M.S., Staal, A., van der Bolt, B., Flores, B.M., Bathiany, S., Scheffer, M., 2016. What do you mean, 'tipping point'? Trends Ecol. Evol. 31, 902–904.

van Tussenbroek, B.I., Hernandez-Arana, H.A., Rodriguez-Martinez, R.E., Espinoza-Avalos, J., Canizales-Flores, H.M., Gonzalez-Godoy, C.E., Barba-Santos, M.G., Vega-Zepeda, A., Collado-Vides, L., 2017. Severe impacts of brown tides caused by Sargassum spp. on near-shore Caribbean seagrass communities. Mar. Poll. Bull. 122, 272–281.

Wang, M., Hu, C., 2016. Mapping and quantifying Sargassum distribution and coverage in the Central West Atlantic using MODIS observations. Remote Sens. Environ. 183, 350–367.

Wang, M., Hu, C., 2017. Predicting *Sargassum* blooms in the Caribbean Sea from MODIS observations. Geophys. Res. Lett. 44, 3265–3273.

Wang, L.-C., Jin, F.-F., Wu, C.-R., Hsu, H.-H., 2017. Dynamics of upwelling annual cycle in the equatorial Atlantic Ocean. Geophys. Res. Lett. 44, 3737–3743.

Wang, M., Hu, C., 2018. Outlook of 2018 Sargassum blooms in the Caribbean Sea. University of South Florida Optical Oceanography Lab, December 30 2018.

Wang, M., Hu, C., Barnes, B.B., Mitchum, G., Lapointe, B., Montoya, J.P., 2019. The great Atlantic *Sargassum* belt. Science 365 (6448), 83–87.

Wang, M., Hu, C., Barnes, B., 2019. Sargassum density and coverage using Moderate Resolution Imaging Spectroradiometer (MODIS) satellite data from 2001-01-01 to 2018-12-31 (NCEI Accession 0190272). NOAA National Centers for Environmental Information. Dataset. https://accession.nodc.noaa.gov/0190272. Accessed [20 August, 2019].

Webb, R.S., Werner, F.E., 2017. Explaining extreme ocean conditions impacting living marine resources [in "Explaining Extreme Events of 2016 from a Climate Perspective"]. Bull. Am. Meteorol. Soc. 98 (12), S7–S10. https://doi.org/10.1175/BAMS-D-17-0265.1.

Webster, R.K., Linton, T., 2013. Development and implementation of *Sargassum* early advisory system (SEAS). Shore and Beach 81, 1–6.

Weingartner, T.J., Weisberg, R.H., 1991. A description of the annual cycle in sea surface temperature and upper ocean heat in the equatorial Atlantic. J. Phys. Oceanogr. 21 (1), 83–96.

Weisberg, R., Tang, T., 1985. On the response of the equatorial thermocline in the Atlantic Ocean to the seasonally varying Trade winds. J. Geophys. Res. 90 (C10), 7117–7128. https://doi.org/10.1029/JC090iC04p07117.

Weisberg, R.H., Colin, C., 1986. Equatorial Atlantic Ocean temperature and current variations during 1983 and 1984. Nature 322, 240–243.

Weisberg, R., Tang, T., 1990. A linear analysis of equatorial atlantic ocean thermocline variability. J. Phys. Oceanogr. 20 (12), 1813–1825. https://doi.org/10.1175/1520-0485(1990) 020<1813:ALAOEA>2.0.CO;2.

Wells, R.J.D., Rooker, J.R., 2004. Spatial and temporal patterns of habitat use by fishes associated with *Sargassum* mats in the northwestern Gulf of Mexico. Bull. Mar. Sci. 74, 81–99.

Winston, J.E., Gregory, M.R., Stevens, L.M., 1997. Encrusters, epibionts, and other biota associated with pelagic plastics: A review of biogeographical environmental, and conservation issues. In: Coe, J.M., Rogers, D.B. (Eds.), Marine Debris: Sources, Impact and Solutions. Springer-Verlag, New York, Inc.

Witherington, B., Hirama, S., Hardy, R., 2012. Young sea turtles of the pelagic *Sargassum*-dominated drift community: habitat use, population density, and threats. Mar. Ecol. Prog. Ser. 463, 1–22.

Wunsch, C., Heimbach, P., Ponte, R., Fukumori, I., 2009. The global general circulation of the ocean estimated by the ECCO-consortium. Oceanography 22, 88–103.

Data web sites accessed in order of appearance in text

NAO index: NOAA's Climate Prediction Center (https://climatedataguide.ucar.edu/climate-data/hurrell-north-atlantic-oscillation-nao-index-pc-based).
HYCOM model: (https://www.hycom.org/).
ICHTHYOP model: (www.ichthyop.org/).

ECCO2 Cube 92 model: (https://ecco.jpl.nasa.gov/drive/files/ECCO2/cube92_latlon_quart_90S90N/).

Sargassum density and coverage using Moderate Resolution Imaging Spectroradiometer (MODIS) satellite data from 2001-01-01 to 2018-12-31: (https://accession.nodc.noaa.gov/0190272).

NCEP reanalysis and GODAS current data: (http://www.esrl.noaa.gov/psd/).

Cross-Calibrated Multi-Platform Ocean Surface Wind Vector L3.0 First-Look Analyses. Ver. 1: (10.5067/CCF30-01XXX).

OSCAR current data: https://www.esr.org/research/oscar/.

Global Drifter Program data: (https://www.aoml.noaa.gov/phod/gdp/), (10.25921/7ntx-z961).

NOAA World Ocean Atlas WOA18 data: (https://www.nodc.noaa.gov/OC5/woa18/).

Update

Progress in Oceanography

Corrigendum

Corrigendum to "The establishment of a pelagic *Sargassum* population in the tropical Atlantic: Biological consequences of a basin-scale long distance dispersal event" [Progr. Oceanogr. 182 (2020) 102269]

Elizabeth M. Johns[a,*], Rick Lumpkin[a], Nathan F. Putman[b], Ryan H. Smith[a], Frank E. Muller-Karger[c], Digna T. Rueda-Roa[c], Chuanmin Hu[c], Mengqiu Wang[c], Maureen T. Brooks[d], Lewis J. Gramer[a,e], Francisco E. Werner[f]

[a] Atlantic Oceanographic and Meteorological Laboratory, National Oceanic and Atmospheric Administration, Miami, FL 33149, USA
[b] LGL Ecological Research Associates, Inc., Bryan, TX 77801, USA
[c] College of Marine Science, University of South Florida, St. Petersburg, FL 33701, USA
[d] University of Maryland Center for Environmental Science, Horn Point Laboratory, Cambridge, MD 21613, USA
[e] Cooperative Institute for Marine and Atmospheric Studies, Rosenstiel School of Marine and Atmospheric Science, University of Miami, Miami, FL 33149, USA
[f] NOAA Fisheries, 1315 East-West Highway, Silver Spring, MD 20910, USA

The authors regret that there is an error in the colour key for Fig. 16. The units for this figure should be $10^{-5}\,\text{s}^{-1}$ rather than $10^5\,\text{s}^{-1}$.

The authors would like to apologise for any inconvenience caused.